

CELL BIOLOGY

Physical determinants of bipolar mitotic spindle assembly and stability in fission yeast

Robert Blackwell,^{1,2} Christopher Edelmaier,¹ Oliver Sweezy-Schindler,¹ Adam Lamson,¹ Zachary R. Gergely,^{1,3} Eileen O'Toole,³ Ammon Crapo,¹ Loren E. Hough,¹ J. Richard McIntosh,³ Matthew A. Glaser,¹ Meredith D. Betterton^{1,3*}

2017 © The Authors, some rights reserved; exclusive licensee American Association for the Advancement of Science. Distributed under a Creative Commons Attribution NonCommercial License 4.0 (CC BY-NC).

Mitotic spindles use an elegant bipolar architecture to segregate duplicated chromosomes with high fidelity. Bipolar spindles form from a monopolar initial condition; this is the most fundamental construction problem that the spindle must solve. Microtubules, motors, and cross-linkers are important for bipolarity, but the mechanisms necessary and sufficient for spindle assembly remain unknown. We describe a physical model that exhibits *de novo* bipolar spindle formation. We began with physical properties of fission-yeast spindle pole body size and microtubule number, kinesin-5 motors, kinesin-14 motors, and passive cross-linkers. Our model results agree quantitatively with our experiments in fission yeast, thereby establishing a minimal system with which to interrogate collective self-assembly. By varying the features of our model, we identify a set of functions essential for the generation and stability of spindle bipolarity. When kinesin-5 motors are present, their bidirectionality is essential, but spindles can form in the presence of passive cross-linkers alone. We also identify characteristic failed states of spindle assembly—the persistent monopole, X spindle, separated asters, and short spindle, which are avoided by the creation and maintenance of antiparallel microtubule overlaps. Our model can guide the identification of new, multifaceted strategies to induce mitotic catastrophes; these would constitute novel strategies for cancer chemotherapy.

INTRODUCTION

The mitotic spindle's bipolar organization facilitates faithful genetic inheritance (1, 2). Spindle bipolarity depends on the proper polar organization of microtubules (MTs), which have biochemically distinct plus and minus ends. Spindle assembly typically starts from two nearby centrosomes, both of which nucleate MTs oriented with their plus ends distal. Interactions between these growing MTs, motor proteins, and MT cross-linkers separate the spindle poles (3) until they reach opposite sides of the cell's genetic material. The resulting bipolar MT array is necessary for the proper segregation of sister chromatids, which attach via their kinetochores to a subset of MTs within the spindle structure. MTs that are not attached to kinetochores form the interpolar bundle and are thought to be primarily responsible for the formation and stability of spindle organization.

Kinesin-5 motors, which push spindle poles apart and generate a bipolar spindle, were discovered in yeasts (4–7). Hagan and Yanagida (6) noted that kinesin-5s in fission yeast contribute both to spindle pole separation and to antiparallel interdigitation of MTs that are initially predominantly parallel, an essential structural transition for the establishment of a bipolar spindle in organisms with closed mitosis. After the discovery that kinesin-14s appear to contribute counteracting forces that pull spindle poles together (8), Saunders and Hoyt (8) proposed the “force-balance model,” in which spindle bipolarity arises from the coordination between outward-directed forces from sliding of interpolar MTs that separate spindle poles and inward-directed forces that pull the poles together. Although force-balance ideas had previously been proposed to explain metaphase chromosome positioning (9, 10), Saunders and Hoyt's work appears to be the first force-balance model of the spindle structure. The force-balance picture was supported by

further work in yeasts showing that kinesin-14s can counteract kinesin-5s (11, 12) and since then has been both widely adopted as a conceptual framework (13–22) and used in mathematical models (23–27) of yeast spindles. Quantitative force-balance models were later applied to *Drosophila* spindle assembly (28–31), and the same ideas have more recently been extended to human cells (32). In parallel with work on spindles, force-balance ideas have been studied in reconstituted MT-motor systems (33–45).

Important previous work has modeled aspects of spindle function and chromosome segregation (46, 47) but not the establishment of bipolarity. Previous aspects of spindle function that have been modeled mathematically include spindle elongation and force balance (27, 28, 30, 48–50), the formation and maintenance of antiparallel MT overlaps (35, 36, 51, 52), MT bundling and sliding (26, 53–58), spindle pole focusing (29, 49, 59, 60), spindle movements and positioning (44, 61–66), spindle length and shape (25, 26, 31, 67–71), and spindle assembly (53, 54, 69, 72–74). Integrated experiments and modeling to study spindle length and kinetochore motility, congression, and segregation in preformed budding- and fission-yeast spindles (23–26, 75–77) have shown how the proper MT length distribution and kinetochore attachments are set up in the assembled spindle. However, previous models have assumed an already-bipolar structure, the most fundamental construction problem that the spindle must solve.

Our aim was to develop a physical model for *de novo* formation of a three-dimensional bipolar spindle, starting from a monopolar initial condition. We have used biophysical modeling and quantification of spindle assembly in a cell type that is both relatively simple and amenable to experimental modification, the fission yeast *Schizosaccharomyces pombe*. This organism has previously been studied in enough detail to allow formulation of a realistic model (78, 79); it is small enough that detailed three-dimensional simulations are computationally tractable (80); it is amenable to the genetic manipulation and quantitative experiments needed to parameterize the model (5, 6, 11, 19, 20, 22, 81–98); and the cell contains only three chromosomes whose separate motions can be imaged. Unlike the situation in budding yeast, the mitotic

¹Department of Physics, University of Colorado, Boulder, CO 80309, USA. ²PULS Group, Department of Physics and Cluster of Excellence: Engineering of Advanced Materials, Friedrich-Alexander University Erlangen-Nürnberg, Nagelsbachstr. 49b, Erlangen, Germany. ³Department of Molecular, Cellular, and Developmental Biology, University of Colorado, Boulder, CO 80309, USA.

*Corresponding author. Email: mdb@colorado.edu

spindle of *S. pombe* shows important similarities to that of metazoans: Spindle assembly begins in mitotic prophase, and kinetochores attach multiple MTs.

A major outstanding question is which functions of the numerous spindle molecules are sufficient for spindle formation. This question has been difficult to answer because the spindle is highly redundant: Many proteins are not individually necessary, and cells may compensate for a single-gene deletion by up- or down-regulating other spindle components (99). Because centrosomes (100) and chromosome-MT attachments (89, 101) are dispensable for spindle assembly, the key ingredients for spindle bipolarity appear to be dynamic MTs, motors, and cross-linkers (102). Cross-linkers appear to play a key role in reconstitution experiments, where kinesin-5 and kinesin-14 motors can generate stable antiparallel MT overlaps only with the addition of a passive cross-linker (37).

Here, we have sought to determine the minimal ingredients necessary for a computational model that generates spindle bipolarity, the key processes that lead to bipolar spindle assembly, and the characteristic ways in which spindle assembly can fail. We have found that dynamic MTs, plus end- and minus end-directed cross-linking motors, and passive cross-linkers are sufficient to robustly self-assemble a bipolar spindle. MT antiparallel overlaps are the key structural element, allowing both assembly and stability of a bipolar spindle. Defects in creating or sustaining antiparallel MT overlaps trap the spindle in states that prevent full assembly. If the spindle is unable to resolve the initially oblique contacts between MTs from opposite centrosomes [called spindle pole bodies (SPBs) in yeasts] into antiparallel overlaps, it becomes trapped as a persistent monopole. If SPB separation occurs without maintenance of antiparallel overlaps, the spindle breaks, either into an X shape with oblique MT-MT contacts (103) or into two separated asters. If spindle elongation is compromised, the spindle remains short (19). Our analysis highlights the particular role of passive cross-linkers, which maintain antiparallel overlaps on which motors can act and promote stabilization of MTs in antiparallel bundles.

RESULTS

Model

We distilled the many overlapping roles played by MT-associated motors and cross-linkers into a set of functions, each manifest in our model as a single molecular species. Only three molecular activities are needed for our model to robustly generate a stable antiparallel MT bundle starting from two side-by-side SPBs (Fig. 1). Plus end-directed cross-linking motors represented by kinesin-5s, previously found to be essential for spindle bipolarity, exert sliding forces between antiparallel MTs (Fig. 1A) (5, 6, 100, 104, 105). We incorporated the remarkable context-dependent direction switching of yeast kinesin-5s (106–110) into our model. Minus end-directed cross-linking motors represented by kinesin-14s promote MT bundling and exert forces that oppose SPB separation (11, 26, 111). Passive cross-linkers, represented by PRC1 (protein regulator of cytokinesis 1)/Ase1-like proteins, promote MT bundling and act as brakes on SPB separation (83, 97, 112, 113) and preferentially bind to antiparallel MT overlaps (112). In our model, motors and cross-linkers move with force-dependent kinetics, and bound motors/cross-linkers exert spring-like forces if stretched/compressed away from their rest length (see Materials and Methods).

Fission yeast uses closed mitosis (in which the spindle forms within an intact nucleus), and there are only relatively small deformations of the nuclear envelope in early mitosis; therefore, we model the nuclear

envelope as a sphere of fixed size (Fig. 1B). SPBs, the yeast centrosomes, are represented as thin disks that are mobile within the nuclear envelope but remain confined to the spherical nuclear envelope throughout all simulations. Fourteen MTs per SPB are nucleated with their minus ends tethered to the SPBs (80) in all simulations and undergo dynamic instability (Fig. 1C). Because fission-yeast mitotic MTs are much shorter than the MT persistence length, we model MTs as rigid rods. The MTs experience forces from motors/cross-linkers, tethering to the SPBs, random thermal kicks, and steric interactions with each other and the nuclear envelope (see Materials and Methods). MTs undergo plus-end dynamic instability, characterized by growing and shrinking states and stochastic switches between them. MTs are stabilized by cross-linking (85).

Because spindle assembly can occur in the absence of centrosomes (101) and fission-yeast mutants defective in kinetochore-MT attachments can still assemble bipolar spindles (89, 92, 98), we have neglected any mechanical contributions of chromosomes. The effects of kinetochore-MT attachments on MT dynamics (23, 25, 114) are implicitly modeled through our optimization of MT dynamics for spindle stability. We use a hybrid Brownian dynamics–kinetic Monte Carlo simulation scheme, as previously described (115–119). Bipolar spindles robustly form (Fig. 1D) and exhibit a time course of SPB separation, a fraction of MTs in the inter-polar bundle, and a structure similar to that found in cells (Fig. 1, E and F).

Parameters and optimization

We used literature data and our own measurements to fix model parameters (see Materials and Methods, the Supplementary Materials, tables S1 and S2, and fig. S1). For the vast majority of model inputs, we used the values from published measurements (see tables S1 and S2). However, for a small number of parameters, published work suggested ranges, not precise values (see table S3). These poorly constrained model inputs were the parameters that describe how MT dynamic instability is altered by motors and cross-linkers, the number of active kinesin-5, kinesin-14, and cross-linker molecules, and the sensitivity of unbinding to applied load for each molecular species (table S3). Using our initial estimates for these less-certain parameters (tables S1 and S2), our model successfully formed bipolar spindles in 62% of simulation runs ($n = 384$), indicating that the model could successfully form spindles in many cases. However, we noticed that some structural features of these model spindles did not correspond well to spindle structure measured by electron tomography (84, 120). Therefore, we used measurements of spindle properties by light microscopy (using 864 spindle length measurements from 16 cells) and spindle tomograms (using MT length, pairing length, and angle distributions from three tomograms) (Figs. 1F and 2) and used these data to optimize the poorly constrained parameters (see the Supplementary Materials). We defined an objective function that quantifies how well simulations of a given parameter set match the data. Optimization using the particle swarm algorithm (121) increased the value of our objective function from a mean of 0.032 for the initial parameter estimates to an average maximum of 0.12 and increased the fraction of simulation runs that formed spindles to 83%. The Kolmogorov-Smirnov test comparing experimental and model distributions of spindle length and structural parameters (see Fig. 2, C, E, and F, Materials and Methods, and the Supplementary Materials) yielded P values of approximately 0.1, indicating that the distributions are statistically similar.

By examining the ranges of parameters found in the most successful parameter sets during model optimization, we learned which parameters must be more tightly constrained and which can vary more

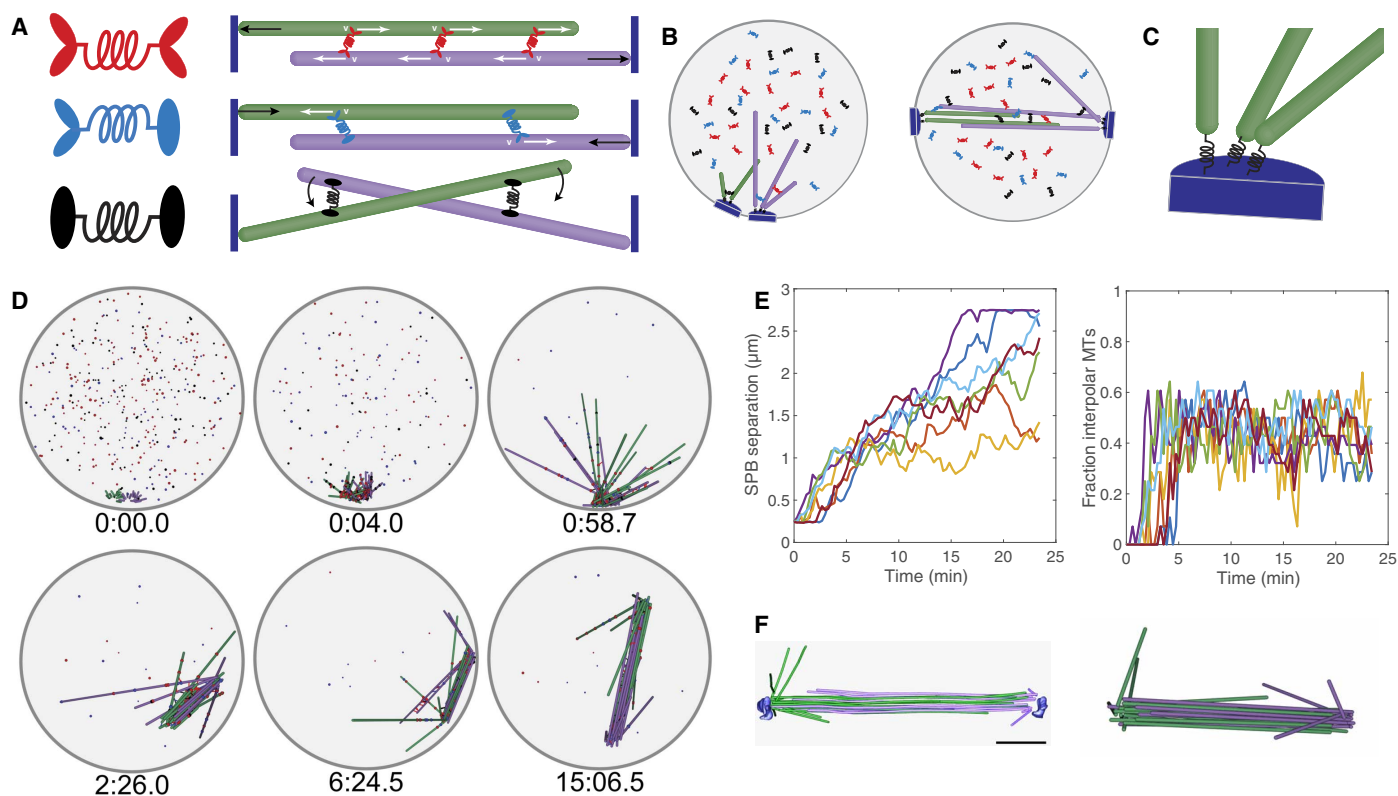


Fig. 1. Overview of spindle assembly model. (A) Schematic of motor and cross-linker effects on MTs. In the schematics, double ovals indicate motor heads, and single ovals indicate passive MT binding domains. Red, kinesin-5 motors; blue, kinesin-14 motors; black, passive cross-linkers. MTs (green and purple) are colored according to their SPB (blue) attachment: Green MT minus ends are tethered to the left SPB and purple MT minus ends are tethered to the right SPB. Kinesin-5 motors promote antiparallel MT sliding and spindle elongation. Kinesin-14 motors promote MT alignment and spindle shortening. Passive cross-linkers promote MT alignment and bundling and favor cross-linking antiparallel MTs. (B) Model schematic. The nuclear envelope (gray sphere) contains mobile but membrane-bound SPBs (blue). MTs (green and purple) are tethered to SPBs at their minus ends. Kinesin-5s (red), kinesin-14s (blue), and cross-linkers (black) diffuse within the volume enclosed by the nuclear envelope and can attach to and move along MTs. (C) Schematic of SPBs and MT minus ends. MTs are attached via springs (black). (D) Image sequences of spindle assembly simulation, rendered from a three-dimensional simulation. Times shown are in minutes and seconds. Initially, the SPBs are adjacent and MTs are short ($t = 0$). Colored spheres indicate motors and cross-linkers, which initially diffuse in the nucleoplasm. A bipolar spindle forms, elongates, and remains stable through the end of the 15-min simulation. (E) Spindle assembly results, shown as SPB separation (left) and fraction of MTs in the inter-polar bundle (right) as a function of time for seven simulations. (F) Comparison of fission-yeast spindle obtained through electron tomography (left) and simulation model (right).

widely and still allow bipolar spindle assembly (table S3). Spindle assembly was relatively insensitive to the specific changes to MT growth speed and shrinking speed by motors and cross-linkers near MT plus ends but appeared to require a large decrease in the catastrophe frequency by a factor ≥ 10 and an increase in the rescue frequency by a factor ≥ 18 . This suggested that stabilization of MTs within bundles in the spindle plays a key role in spindle assembly, as discussed further below. We found that the stabilization length (the length from MT plus ends within which motors and cross-linkers stabilize MT dynamics) was optimally 12 to 25.5 nm or 1.5 to 3.5 tubulin dimers. This length is consistent with local effects on dynamics of small numbers of motors and microtubule-associated proteins (MAPs) near MT plus ends. Although mass spectrometry has measured the numbers of kinesin-5s, kinesin-14s, and cross-linkers per fission-yeast mitotic cells to be ≥ 1000 (93), we found that the model performed best when the numbers of these components in the nucleus are ~ 100 to 200. This difference from the mass spectrometry results could occur if not all molecules are localized to the nucleus or are active during mitosis. We also found interesting effects of the sensitivity of motor and cross-linker unbinding

to the force applied to the cross-linked molecule, which we investigated in more detail and discuss below.

We noticed that the results of our optimization tended to give a spindle length distribution that did not match the experimental data well. In parallel work, we had found that steady-state spindle length varies significantly with the ratio of kinesin-5 to kinesin-14 motors (discussed further below). Therefore, we varied the kinesin-5 and kinesin-14 motor numbers together to improve the spindle length distribution. These small changes to the parameters gave the best “wild-type” parameter set for which every simulation run led to a bipolar spindle (Fig. 1, tables S1 and S2, and video S1).

Single perturbations

Having established a wild-type parameter set that robustly leads to a well-formed bipolar spindle in our model, we compared our model to established experimental results. We first studied the model equivalent of single-gene deletions by setting the number of active kinesin-5s, kinesin-14s, or cross-linkers to zero while fixing all other parameters (see Materials and Methods and the Supplementary Materials).

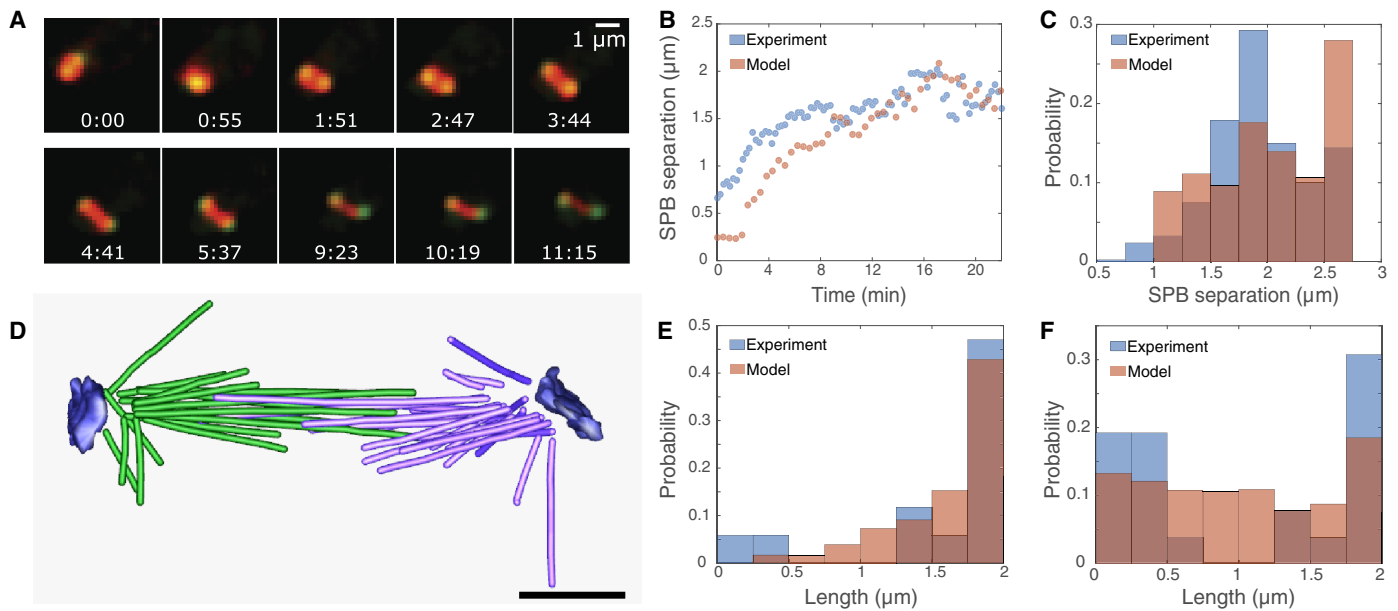


Fig. 2. Spindle measurements used to optimize model parameters. (A to C) Spindle length. (A) Time lapse images of spindle assembly and elongation. Confocal images show *S. pombe* spindles with mCherry-labeled MTs (red) and green fluorescent protein-labeled SPBs (green). Times shown are in minutes and seconds; dimming is a result of photobleaching. (B) SPB separation as a function of time from three-dimensional experimental measurements on one cell (blue) and one model simulation (orange). (C) Distributions of SPB separation of metaphase spindles from experimental measurements (blue) and simulation (orange). (D to F) Spindle structural characteristics from electron tomograms. (D) Tomographic reconstruction of a 1.04- μm -long fission-yeast spindle. (E) Interpolar MT length distributions for MTs in a 2.15- μm -long spindle determined from experimental measurements (blue) and simulation (orange). (F) MT length distributions for all MTs in a 2.15- μm -long spindle determined from experimental measurements (blue) and simulation (orange).

Consistent with fission-yeast genetics, kinesin-5 deletion abolishes bipolar spindle assembly (5, 6), whereas kinesin-14 or cross-linker deletion does not (Fig. 3, A and B, and fig. S2) (11, 83). Consistent with the force-balance picture that kinesin-14 exerts forces that bring SPBs together and oppose spindle elongation (8, 11, 12), kinesin-14 deletion leads to more rapid SPB separation and longer spindles than when kinesin-14 is present. Consistent with recent findings that passive cross-linkers act as brakes on MT separation and help maintain antiparallel overlaps (97, 113), cross-linker deletion also leads to faster spindle elongation and longer spindles. In the wild-type model, the average fraction of interpolar MTs was about 0.5 but was half that value for the models with kinesin-14 or cross-linkers deleted (Fig. 3, A and B). This suggests that the known MT bundling activities of kinesin-14s (26) and cross-linkers (83, 97, 113, 122) help stabilize antiparallel overlaps in our model.

Stabilization of cross-linked spindle MTs by the cytoplasmic linker-associated protein (CLASP) is essential for spindle formation in fission yeast (85) and is included in our model through the stabilization of MT dynamics upon cross-linking. To model CLASP deletion, we turned off this stabilization of MT dynamics by motors and cross-linkers. This alteration abolishes spindle assembly: SPBs do not separate, and the interpolar MT fraction remains near zero (Fig. 3A and fig. S3), suggesting that the stabilization of MT dynamics in bundles is essential for maintaining MT antiparallel overlaps and for the assembly of a bipolar spindle. Our simulation runs that mimicked these four single-gene deletions demonstrate that our model not only matches quantitative measurements of wild-type *S. pombe* cells but also reproduces results on mutants that were not used to optimize the model. Therefore, we proceeded with confidence to study additional perturbations that are more difficult to achieve experimentally.

Load-induced unbinding.

Next, we varied the sensitivity of unbinding when stretched for each of the three MT-cross-linking species under consideration. Because force-induced unbinding is known to be important in other cytoskeletal systems (123), we reasoned that it might affect spindle assembly (Fig. 3, C and D, and figs. S4 to S6). The unbinding load sensitivity is controlled by the parameter λ , which controls how motor or cross-linker spring extension affects its binding and unbinding. To maintain proper Boltzmann statistics, the on and off rates are altered by the exponential of the energy change that occurs upon binding or unbinding: $k_{\text{off}} \propto \exp(\lambda E)$ and $k_{\text{on}} \propto \exp(-(1 - \lambda)E)$, where λ is the unbinding load sensitivity and E is the elastic energy stored in the motor or cross-linker spring when bound to two MTs (eqs. S19 and S23). When $\lambda = 0$, the elastic energy has no effect on unbinding; it only has an effect on binding. At the other limit, when $\lambda = 1$, the unbinding is maximally sensitive to load, but binding is load-independent. Bipolar spindle assembly is optimal when kinesin-5 has “Goldilocks” load sensitivity, that is, when kinesin-5 motors have intermediate sensitivity to unbinding when loaded. When $\lambda = 0$ for kinesin-5s, the unbinding rate of kinesin-5 motors is constant, even when they are highly stretched. As a result, force production by kinesin-5s is high and spindles are longer, on average, in the model than observed in cells. As the kinesin-5 unbinding load sensitivity increases, the rate of unbinding of highly stretched motors increases. This limits the force that kinesin-5s can generate to separate SPBs and correspondingly decreases spindle length. Varying kinesin-14 and cross-linker load sensitivity is significant only when this parameter is near zero: Thus, kinesin-14s and cross-linkers unbind at a constant rate, even when highly stretched, and oppose kinesin-5 SPB elongation too strongly, leading to short spindles. The unbinding load sensitivities were among the poorly constrained parameters varied in

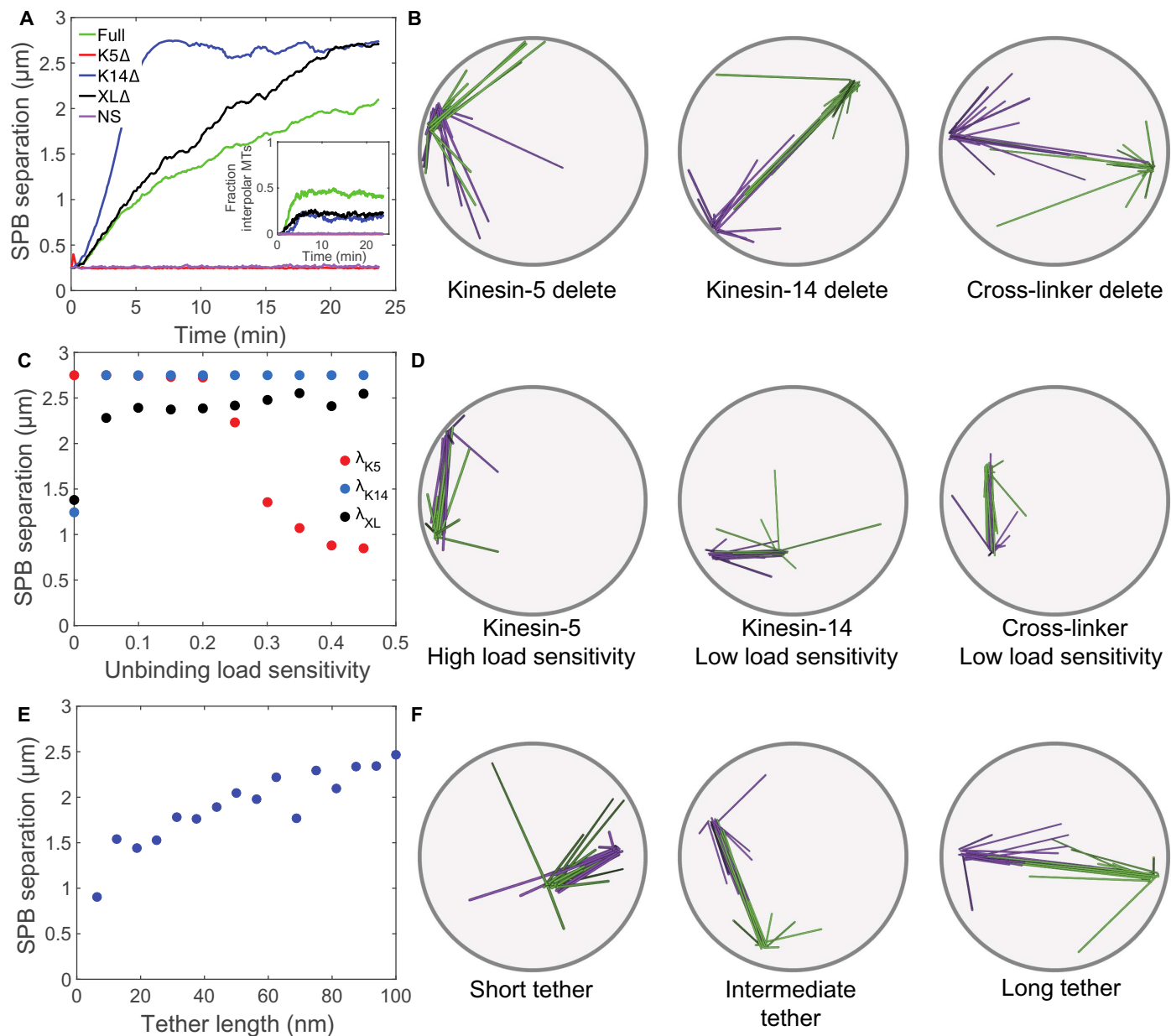


Fig. 3. Effects of single model perturbations on spindle assembly. Results in plots represent averages of 16 simulations; for individual simulation traces, see figs. S2 to S7. Left, plots; right, simulation snapshots. **(A and B)** Effects of individual kinesin-5, kinesin-14, and cross-linker deletions and loss of MT dynamics stabilization by motors and cross-linkers. Full (green), best wild-type model; K5Δ (red), kinesin-5 motors removed from model; K14Δ (blue), kinesin-14 motors removed from model; XLΔ (black), passive cross-linkers removed from model; NS (purple), stabilization of MT dynamics by motors and cross-linkers removed from model. Spindle assembly is abolished by kinesin-5 deletion and removal of dynamics stabilization. **(C and D)** Effects of altering sensitivity to force-induced unbinding of kinesin-5 (K5), kinesin-14 (K14), and cross-linker (XL). **(E and F)** Effects of altering SPB-MT tether length. Spindles are unable to elongate when tethers are short. Note that when SPBs do not appear on the perimeter of the circle shown; they remain attached to the nuclear envelope at some point above or below the sphere's equator.

our optimization, and the values found are consistent with this analysis (table S3).

MT-SPB tether spring length.

For the spindle to transition from monopolar to bipolar, MTs that initially make oblique contacts must undergo large rotations to point toward the other SPB. Therefore, we asked whether varying the rest length of the tether springs connecting MT minus ends to SPBs (124, 125) might affect establishment of spindle bipolarity (Fig. 3, E and F, and fig. S7).

We found that spindle length varies approximately linearly with tether length. When the tethers are too short, MT rotation to point toward the other SPB decreases, and spindle length and the fraction of MTs in the inter-polar bundle decrease (video S2). This result suggests that the MT-SPB attachments must be both sufficiently tight and strong to maintain a physical connection between them (19, 126) and sufficiently rotationally unconstrained to allow free MT rotational diffusion (91) in order for spindles to assemble successfully. If MTs are more

Downloaded from <http://advances.sciencemag.org/> on January 20, 2017

rotationally constrained by a short tether spring, antiparallel MT overlaps and, therefore, force generation appear to be limited.

Kinesin-5 bidirectionality

Kinesin-5 motors in both budding and fission yeasts have the surprising ability to reverse direction as a function of MT binding and polarity (106, 110). We therefore examined the effects of kinesin-5 direction reversal on model spindle assembly (Fig. 4 and fig. S8). In our wild-type model, kinesin-5s move toward MT plus ends only when both heads are bound to a pair of antiparallel MTs. The motors move toward minus ends when both heads are bound to parallel MTs or bound with a single head, consistent with experimental findings (106, 110). Altering this direction switching leads to defects in model spindle formation. If we make kinesin-5s minus end-directed only on parallel MTs, spindles form but are unable to elongate fully (Fig. 4, A and B). Making kinesin-5 minus end-directed only for singly attached heads, or removing the minus end-directed motion entirely, completely abolishes bipolar spindle assembly, qualitatively similar to the kinesin-5 deletion (video S3).

These results suggested the possibility that yeast kinesin-5s must be properly localized for spindle assembly and that kinesin-5 bidirectionality enables proper localization. To test this hypothesis, we first measured

kinesin-5 localization in monopolar spindles in which SPBs were adjacent. We averaged the distance of kinesin-5 motors from the SPB when bound to MTs from that SPB (Supplementary Materials). In the wild-type model, kinesin-5s localize near the SPB (Fig. 4C). When kinesin-5s are minus end-directed only on parallel MTs but plus end-directed when singly attached, the localization shifts even more toward the SPB. When kinesin-5s are plus end-directed on single MTs or always plus end-directed, the localization shifts markedly away from the SPBs toward MT plus ends. Kinesin-5s localized to MT plus ends are not well positioned to stabilize antiparallel MT overlaps and exert forces that separate SPBs because motors near MT tips are more likely to interact only transiently with the plus ends of MTs from the other SPB before unbinding. On the other hand, minus end-directed motility on parallel bundles positions kinesin-5s where they can attach to MTs from the other SPB and exert force, but the strong SPB localization suggests that, in this case, the motors may become stuck at the SPBs and are unable to redistribute to the interpolar bundle and generate force. In the full-bidirectional kinesin-5 model, motors are poised near the SPBs to establish and stabilize antiparallel overlaps but can also redistribute throughout the spindle. We confirmed this understanding by measuring kinesin-5 localization in bipolar spindles $<1.3 \mu\text{m}$ long in the wild-type and parallel-minus

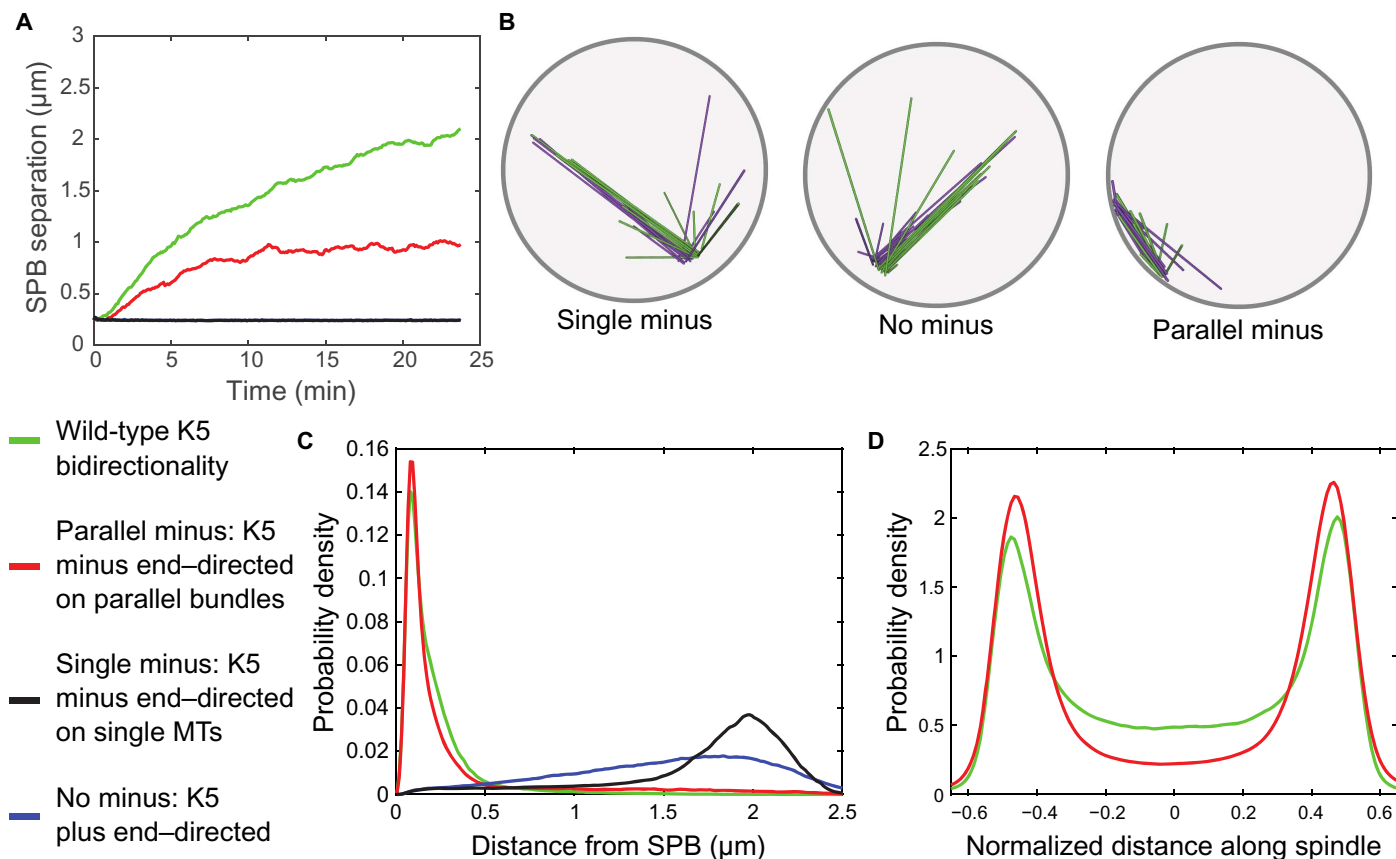


Fig. 4. Effects of kinesin-5 bidirectionality on spindle assembly and motor localization. Results in plots represent averages of 16 simulations; for individual simulation traces, see fig. S8. Lower left: “Wild type” means that kinesin-5s are minus end-directed when cross-linking parallel MTs or bound to a single MT and plus end-directed when cross-linking antiparallel MTs. “Parallel minus” means that kinesin-5s are minus end-directed only when cross-linking parallel MTs and plus end-directed otherwise. “Single minus” means that kinesin-5s are minus end-directed only when attached with one head to a single MT and plus end-directed otherwise. “No minus” means that kinesin-5s are always plus end-directed. **(A)** SPB separation as a function of time. Compared to the wild-type model, the parallel-minus model shows shorter spindles. The no-minus and single-minus models abolish spindle assembly. **(B)** Simulation snapshots. **(C)** Average kinesin-5 motor localization on monopolar spindles. In the wild-type and parallel-minus models, kinesin-5s are localized near the SPBs. In the single-minus and no-minus models, the kinesin-5s are localized distal to the SPBs. **(D)** Average kinesin-5 localization on short ($\sim 1 \mu\text{m}$ long) spindles. Both wild-type and parallel-minus models show kinesin-5 localization near the SPBs, but the parallel-minus model shows decreased kinesin-5 localization in the center of the spindle.

motility models (Fig. 4D). Both types of motility lead to kinesin-5s localized throughout the spindle, with peaks near the SPBs, consistent with experimental results (6). Notably, the kinesin-5s in the parallel-minus motility show enhanced SPB localization and a lower concentration near the center of the spindle, approximately half that of the wild-type model. This suggests that only in our wild-type model do kinesin-5s have both sufficient pole localization to generate force that separates SPBs and the ability to redistribute to the center of the spindle to sustain the force needed to fully elongate the spindle.

Combined perturbations

A strength of computational modeling is the ease and speed with which multiple perturbations can be studied. We first examined the combined deletion of kinesin-5 and kinesin-14. In *S. pombe*, deletion or inactivation of kinesin-5 alone abolishes spindle formation and is lethal, but simultaneous deletion of kinesin-14 rescues viability (11, 94). We first removed kinesin-5 and kinesin-14, keeping all other parameters fixed; in this case, spindle formation does not occur. We hypothesized that cells might compensate for the loss of important mitotic motors by altering MT dynamics and cross-linker number to allow spindles to form, so we increased the cross-linker number by a factor of 2.3 to 250 molecules and increased the rescue frequency. We chose to vary the rescue frequency because, in our optimized parameter set, the rescue frequency stabilization factor due to MT bundling was the largest in magnitude and apparently the most important of the four dynamic instability parameters. For the smaller number of MT-bundling molecules present in cross-linker-only spindles (250 cross-linkers versus 374 motors and cross-linkers in the reference parameter set), we reasoned that a higher rescue frequency might better help maintain antiparallel MT contacts. Consistent with our expectation, these changes to the model allowed spindle assembly with cross-linker molecules only (Fig. 5A and table S4). In our model, increasing the MT rescue frequency is crucial to maintain antiparallel MT overlaps and spindle bipolarity with cross-linkers only present. The fraction of simulations for which bipolar spindle assembly occurs increases with increasing MT rescue frequency, from about 3% success for a rescue frequency of 0.55 per min to 20 to 30% success for a rescue frequency around 1.5 per min. In failed simulations, the spindles typically form X spindles, a defective spindle state, as discussed further below. We also found, surprisingly, that successful cross-linker-only spindle formation required decreasing the linkage time at the start of the simulation (during which SPBs are not allowed to move) to zero, allowing initial antiparallel MT contacts to form before MTs grew longer. In short, cross-linker-only spindles can form, but they do so less robustly than when motors play complementary roles. Thus, during evolution, functional spindles could have begun with minimal MT-organizing components and then evolved to become more robust.

Next, we examined the effect of simultaneously varying the concentrations of two of three of our MT-interacting proteins, with other parameters fixed. First, we varied kinesin-14 and cross-linker concentrations together (Fig. 5B, fig. S9, and video S4). As shown in the left panel of Fig. 5B, spindle length is primarily controlled by kinesin-14 number, which decreases as kinesin-14 concentration increases, as observed experimentally (12). Interpolar bundle stability is primarily controlled by the cross-linker number, which becomes larger as cross-linker concentration increases. However, when both kinesin-14 and cross-linker numbers are low, their low combined number leads to spindle instability in which kinesin-5 motors drive SPB separation, but antiparallel MT overlaps cannot be maintained and the spindle breaks

into two separated asters. A similar phenomenon has been observed in spindle reconstitution experiments (37).

Next, we varied kinesin-5 and kinesin-14 concentrations together (Fig. 5C, fig. S10, and videos S5 and S6). Consistent with published results (8, 11, 12), we find that decreasing the number of kinesin-5s has a larger effect on spindle length the more the number of kinesin-14s is increased. Therefore, kinesin-5 depletion combined with kinesin-14 overexpression leads to a larger disruption of spindle assembly than what occurs for either perturbation alone. Previous work showed that kinesin-5 overexpression can induce premature spindle elongation in budding yeast (12). Premature spindle elongation is not an effect that we can directly reproduce in the model because we assumed that the nuclear envelope remains spherical and that the SPBs cannot move off the surface of this sphere. However, we estimated parameters for which spindle instability due to premature elongation would occur by measuring the total force exerted on each spindle pole. The physical properties of deformation of fission-yeast nuclear envelopes have been estimated on the basis of the shape of deformed envelopes (127, 128), so we can use these constants and theoretical predictions of the force required to deform membranes sufficiently to produce a membrane tube (see the Supplementary Materials) (129). In Fig. 5C, we have colored the bars representing specific parameter sets red if the average force produced is so large that it would lead to nuclear-envelope deformation and premature elongation. Consistent with expectations of the force-balance model, the ratio of kinesin-5 number to kinesin-14 number is the crucial variable controlling spindle length. If the kinesin-14 number is low, all but the two lowest kinesin-5 numbers are predicted to undergo premature elongation because of unbalanced antiparallel sliding force by kinesin-5s. As the kinesin-14 number increases, this premature-elongation threshold goes up until, for a high kinesin-14 number, only the largest kinesin-5 number would be predicted to lead to premature elongation.

DISCUSSION

Comparison to previous spindle models

As mentioned above, most spindle models have examined specific aspects of spindle function (46, 47) rather than assembly. Here, we compare our work with previous models of *Xenopus* meiotic spindle (53, 54, 69, 72, 73) and human spindle (74) assembly.

The *Xenopus* meiotic spindle assembly modeling work has examined how aspects of MT nucleation, sliding, and clustering contribute to spindle organization (53, 54, 69, 72, 73). The models did not seek to quantitatively match *Xenopus* spindle geometry or structure, examined a few hundred MTs (much less than the $\sim 10^5$ MTs in a *Xenopus* spindle), and were studied in one or two dimensions. An important difference from our work is that each of these models assumed a bipolar structure as an initial condition and thus could not examine the initial establishment of bipolarity. Specific assumptions were made to simplify analysis of the models; for example, MT length was fixed in time (no dynamic instability), and in most cases, all MTs had the same length (53, 54). Later models included more spindle mechanisms, including dynamic MTs with altered dynamics due to motors, explicit cross-linking motors and passive cross-linkers, and multiple nucleation mechanisms that allowed one to study the effects of MT nucleation, dynamic instability, flux, and motors and cross-linkers (69, 72, 73). These models were initialized with fully formed MTs of the same length, which interacted through simplified repulsive and attractive forces.

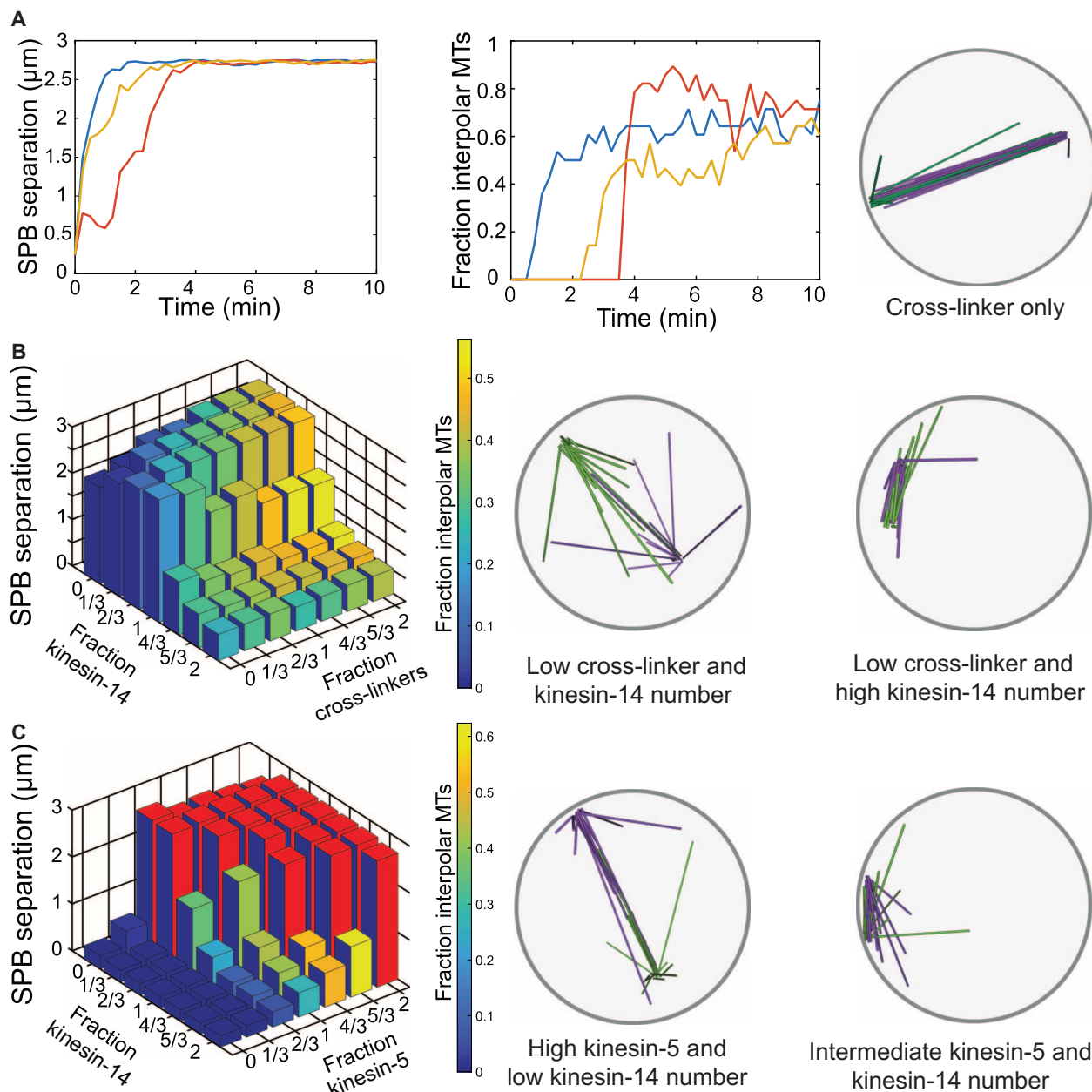


Fig. 5. Model predictions for combined perturbations. (A) Cross-linker-only spindle formation in the model with kinesin-5 and kinesin-14 removed, combined with alterations to cross-linker number, rescue frequency, and linkage time (table S4). Dynamics of SPB separation (left) and inter-polar MT fraction (inset) for four individual simulations (the blue curve represents simulation with a rescue frequency of 0.55 per min and other curves indicate simulations with a rescue frequency of 0.67 per min). Fraction of 32 simulation runs that successfully assembled a bipolar spindle as a function of rescue frequency (center). Error bars are the SE of the mean of a binomial distribution. Spindle snapshot (right). (B) Results of simultaneously varying cross-linker and kinesin-14 number relative to the wild-type model. See fig. S9. Bar height indicates late-time SPB separation, and bar color indicates average fraction of inter-polar MTs for low-force spindles; red bars indicate spindles for which the force on the SPBs is so large that they would become unstable (left). Simulation snapshots (center, right). (C) Results of simultaneously varying kinesin-14 and kinesin-5 numbers relative to the wild-type model. See fig. S10. Bar height indicates late-time SPB separation, and bar color indicates average fraction of inter-polar MTs for low-force spindles; red bars indicate spindles for which the force on the SPBs is so large that they would become unstable (left). Simulation snapshots (center, right).

Important recent work on human spindles incorporated experimental evidence that kinetochore size changes after MT attachment to motivate a new model of chromosome capture by spindle MTs (74). Simulations were initialized with separated centrosomes connected by a constant-length set of spindle MTs. This fully three-dimensional model

based on HeLa cells used 46 chromosomes and 1200 capturing MTs; the MTs were dynamic, stabilized upon kinetochore attachment, and did not sterically interact. In the model, changes in kinetochore size during early mitosis have an important effect in the model of both accelerating kinetochore-spindle attachment and decreasing errors.

Our model development built on the advances of previous work and was focused on different questions. We sought to model the establishment of bipolarity and quantitatively accurate spindle structure in an organism with a small number of MTs. To address these questions, we introduced some new modeling approaches. First, we modeled a fully three-dimensional geometry with a biologically realistic number of spindle MTs. Because steric interactions between MTs may contribute to MT alignment and the establishment of bipolarity, we modeled short-range hard-wall repulsion between MTs rather than neglecting MT-MT interactions or using a spring-like repulsion. We also built on our previous work (115, 116, 118) to compute the statistical mechanics of motor and cross-linker binding and unbinding kinetics accurately, ensuring that detailed balance is maintained at the level of single binding/unbinding events. Finally, we used quantitative comparison of our simulated spindles' length and structure to data from light and electron microscopy to optimize the model's poorly constrained parameters.

Failed states of spindle assembly

We have identified a sequence of key steps required for a bipolar spindle structure to self-assemble from initially adjacent SPBs (Fig. 6). Our work emphasizes the importance of establishing and maintaining MT antiparallel overlaps because these are the key structural elements that allow both assembly and stability of a bipolar spindle. Force-balance ideas are helpful in understanding spindle length, and establishment of a balance of forces requires a suitable bipolar structure that can extend or contract. Therefore, several "failed states" of spindle assembly in our model reflect defects in creating or sustaining antiparallel MT overlaps. We propose that these failed states act as kinetic traps that can be avoided or exited by the proper combinations of MT dynamics and motor and cross-linker activity.

Persistent monopole.

A key first step in spindle assembly is the resolution of initial oblique interactions between MTs from opposite SPBs into antiparallel overlaps with a significant pairing length. If this fails to happen, spindles become trapped as persistent monopoles (Fig. 6B). This typically occurs if antiparallel sliding activity is compromised or if there is too much MT parallel bundling or cross-linking. As seen both in our model (Fig. 3A) and experimentally (5, 6, 130–132), missing or inactive kinesin-5 motors lead to persistent monopoles. An important finding of our work is that kinesin-5 mislocalization can also lead to persistent monopoles (Fig. 3, G and H); in our model, if kinesin-5 motors always move toward MT plus ends, they are not well positioned to create antiparallel overlaps and, therefore, are unable to properly establish antiparallel sliding. A high kinesin-14 or cross-linker number can lead to a persistent monopolar state because the MT cross-linking activity can prevent the establishment of antiparallel MT overlaps (Fig. 5, B and C). Persistent monopoles also occur in cross-linker-only spindles, particularly when parallel MT binding is favored or when the number of cross-linkers is low.

Resolving oblique MT contacts into true antiparallel overlaps may be particularly important for organisms, such as yeasts, for which the SPBs remain in the nuclear envelope during mitosis, because the MTs nucleated from the SPBs point in approximately the same hemisphere with their central axes perpendicular to the envelope (6, 103). For organisms, such as humans, with open mitosis and centrosomes that are often separated at the onset of spindle assembly, initial antiparallel MT overlaps may be easier to create from MTs that grow directly toward the opposite centrosome. However, even in these cells, many oblique

contacts between MTs from opposite centrosomes can occur and must be resolved, suggesting that the mechanisms we identified could contribute to spindle assembly in a range of organisms.

X spindle.

Once initial antiparallel MT overlaps have been established and antiparallel sliding activity begins to push the SPBs apart, the crucial antiparallel overlaps must be maintained or increased. Typically, antiparallel sliding is driven by kinesin-5 motors, but it can also be driven by antiparallel cross-linking coupled to MT growth. If this occurs successfully, the spindle elongates to a metaphase-like structure. If the sliding forces are not coordinated with sufficient antiparallel bundling, the spindle can break into an X spindle (Fig. 6C). Defects in resolving oblique MT contacts into antiparallel overlaps were observed in budding yeast γ -tubulin mutants (103). This work found that the oblique MT contacts allow initial pole separation, but the spindles were unstable, qualitatively consistent with our model observations of X spindles. The X spindle failed state can occur in the model with a low kinesin-14 or cross-linker number because the MT antiparallel overlaps are not maintained as the SPBs separate. X spindles are also the most common failure type of cross-linker-only spindles; cross-linkers often drive the formation of a single parallel bundle containing all MTs from each SPB, which are then linked to MTs from the other SPB in an X.

Separated asters.

Another typical failure of spindle elongation happens when antiparallel sliding occurs, but antiparallel MT overlaps are not maintained, leading to separated asters (Fig. 6D). We might think of the separated asters as analogous to a premature anaphase B, in which SPBs separate and then lose their connections, as has been observed experimentally in budding yeast with overexpressed kinesin-5 motors (12). This often occurs in the model when MTs in antiparallel bundles are not sufficiently stabilized, allowing the antiparallel overlaps to be lost. This is one failure observed when we remove stabilization of MT dynamics in bundles from the model (Fig. 3A). Decreased antiparallel MT bundle stability when kinesin-14 or cross-linkers are deleted (Fig. 3, A and B) can also lead to separated asters. Alterations to MT dynamics that make it difficult to stabilize antiparallel overlaps—particularly low rescue frequency or high shrinking speed—can also lead to separated asters. Separated asters can sometimes be a transient state if MTs are able to reestablish antiparallel contacts and rebuild the interpolar bundles. Avoiding the separated aster state highlights the particular role of cross-linkers in spindle maintenance; they help kinetically trap antiparallel overlaps, maintaining a structure on which motors can act and inducing stabilization of MT dynamics in antiparallel bundles. The preference of cross-linkers for antiparallel MT overlaps, as has been measured (112), is therefore key for spindle assembly.

The maintenance of antiparallel MT arrangements by attachments to kinetochores also likely contributes to maintaining spindle bipolarity and avoiding separated asters, both by maintaining mechanical connections between MTs from opposite SPBs through bioriented chromosomes and by the stabilization of the dynamics of kinetochore MTs. In future work, it would be interesting to investigate whether the mechanical contributions of MT-kinetochore attachments lessen the need for passive cross-linkers in spindle assembly.

Short spindle.

The last observed defect in spindle assembly is the short spindle (Fig. 6E), caused by failure of elongation. Short spindles can be caused by insufficient antiparallel sliding, excess forces bringing the SPBs together, or resistance to elongation. Alterations in the unbinding load sensitivity in

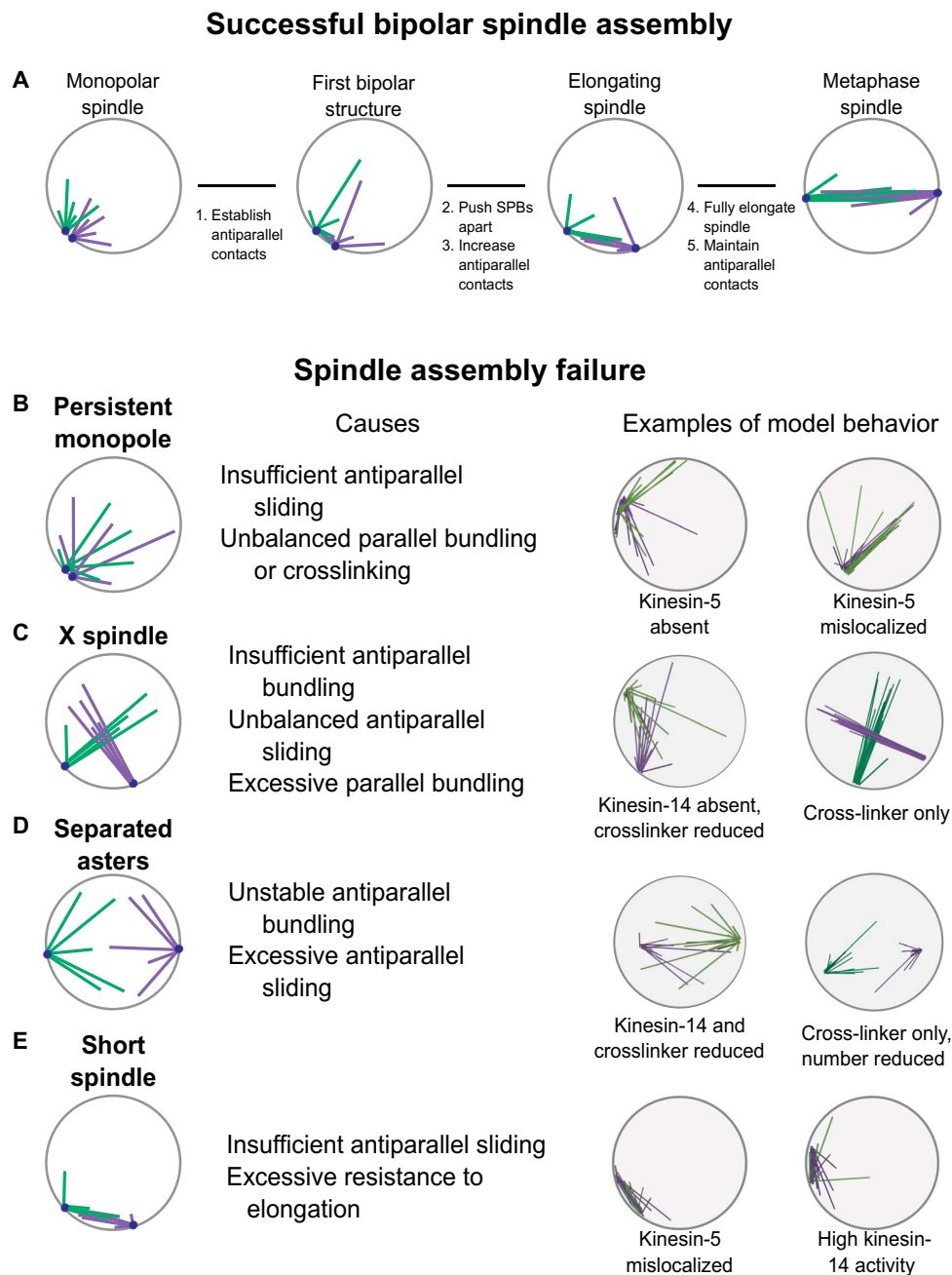


Fig. 6. Successful and failed states of spindle assembly. (A) Successful bipolar spindle assembly requires establishment and maintenance of antiparallel MT overlaps to separate SPBs. (B to E) Failed states of spindle assembly. (B) Persistent monopole state in which SPBs never separate. (C) X spindle in which MTs from separated SPBs experience oblique contacts only. (D) Separated asters in which antiparallel MT bundles have been lost. (E) Short spindle in which spindle elongation is not complete.

our model can lead to short spindles (Fig. 3, C and D). Intriguingly, we found that spindle length scales with the length of the tether linking SPBs to MT minus ends (Fig. 3, E and F) because short tethers make it more difficult for MTs to rotate into configurations that can develop antiparallel overlaps, thereby limiting antiparallel force production. Mislocalized kinesin-5 motors (due to alterations in the direction-reversal model that bias kinesin-5s toward MT plus ends) can also limit antiparallel force production and yield short spindles (Fig. 3, G and H). Finally, changing the relative activity of kinesin-5 and kinesin-14

motors leads to short spindles if kinesin-5 activity is too low and/or kinesin-14 activity is too high (Fig. 5, B and C), as has been observed in budding yeast (12).

Kinesin-5 direction switching.

One of the most intriguing findings is that the bidirectional motion of kinesin-5 motors is necessary for spindle assembly in our model. In particular, the minus end-directed motility of kinesin-5s when singly attached or cross-linking parallel MTs means that they are primarily localized near the spindle poles in both monopolar and bipolar spindles.

This localization positions them properly to stabilize antiparallel MT contacts and exert forces that separate SPBs. Increased localization of kinesin-5s at spindle poles has been observed for fission-yeast (6), *Xenopus* egg extract (130, 133), and mammalian (131, 134) spindles, qualitatively similar to our model results. Although bidirectional motion of the type we model has only been observed for yeast kinesin-5s to date (106–110), there are suggestions that kinesin-5s in other organisms may be affected by the need to correctly localize for spindle assembly. Eg5 is typically considered to be plus end–directed (104, 105, 135–137), whereas the purified *Xenopus* protein can switch between diffusive and directed motility (138). Intriguingly, chimeric proteins in which the kinesin-5 motor domain was replaced with motor domains of other kinesins were not functional for *Xenopus* extract spindle stability (139). Further, Eg5 is transported toward spindle poles by dynein-dynactin in *Xenopus* extract spindles (140). Although this previous work suggested that the poleward transport might indicate an additional function of kinesin-5 motors beyond antiparallel sliding in the spindle midzone (140), our results on kinesin-5 localization suggest another possibility: The poleward transport of Eg5 probably contributes to its antiparallel sliding activity, given that MTs of both polarities are present throughout *Xenopus* extract spindles (141). Therefore, our conclusion about the importance of poleward motility for proper localization of kinesin-5s in the spindle may generalize to organisms beyond yeasts.

Spindle disruption

Currently, the expense and time required to develop chemotherapeutic drugs means that single-molecular targets are typically considered in a “sledgehammer approach” designed to highly perturb one molecule. These drugs are not always successful (142). Even for successful sledgehammer therapies, the mechanism of action is not always understood. Cells can compensate for a single loss by up- or down-regulating other spindle components (99), which can facilitate drug resistance. In the future, our model could be used to optimize failure in spindle assembly and identify candidate targets for chemotherapeutic agents. Our computational model allows large numbers of perturbations to be tested orders of magnitude faster than by experimental work.

MATERIALS AND METHODS

Model design

Our model uses hybrid computational schemes that combine Brownian dynamics and kinetic Monte Carlo simulation. Brownian dynamics govern the motion of physical objects, such as MTs and SPBs (143, 144), by incorporating both deterministic forces/torques due to steric interactions and motors/cross-linkers and random forces/torques due to thermal fluctuations. Kinetic Monte Carlo methods model stochastic events that change the state of molecules in the system, including motor/cross-linker binding/unbinding and MT dynamic instability. We previously used these techniques to model MT-motor mixtures and kinetochore capture (115–119).

The spindle assembly simulation takes place within a sphere of constant shape and diameter that represents the nuclear envelope of fission yeast. Although the nuclear envelope can change shape during spindle formation, its deformations are typically small and appear to be unimportant to spindle formation. The SPBs are thin disks inserted into the nuclear envelope, each with 14 MT nucleation sites (80). Each SPB can move (translate and rotate) within the nuclear envelope because of forces exerted on it by the attached MTs, random thermal forces, and

drag forces from the envelope, which oppose SPB motion (145). To model the initial physical connection of the SPBs via a bridge (95, 96), we held the SPBs fixed while MT and motor/cross-linker dynamics took place for a short SPB linkage time τ_{link} .

MTs were modeled as 25-nm-diameter (146) rigid rods, which interact via nearly hard-core interactions. The MTs diffuse both rotationally and translationally, constrained by the tethering of their minus ends to the SPB (124, 125). MT rotational diffusion about a pivot at the SPB was measured (91), allowing us to correctly compute MT diffusion for any length (119). MT plus-end dynamic instability is described by growing and shrinking speeds and catastrophe and rescue frequencies, which have been measured or estimated (82, 91, 119). MTs switch stochastically between growing and shrinking states. If an MT plus end encounters the nuclear envelope, it experiences force-induced catastrophe, as previously measured (147, 148). Each MT has a minimum length that, if reached, causes the MT to switch to the growing state to maintain a constant MT number.

Our model includes three key protein activities: a kinesin-5–like plus end–directed cross-linking motor (5, 6, 104–110), a kinesin-14–like minus end–directed cross-linking motor (11, 26, 111), and an Ase1/PRC1–like passive cross-linker (83, 97, 112, 113). We determined upper bounds on the number of active molecules of each type from fission-yeast proteomics data (93). Our model includes the alteration of MT dynamics by motors and MAPs. Previous work showed that MT cross-linking recruits CLASP proteins that stabilize MT dynamics (85) and that some motors and cross-linkers bind preferentially to antiparallel MT overlaps (149). We modeled these effects by allowing binding to antiparallel MT pairs to be enhanced and by altering MT dynamics parameters if motors/cross-linkers are present within a certain length from the MT end to stabilize bundled MTs. We note that previous work has found evidence that one budding-yeast kinesin-5 motor, Cin8, destabilizes spindle MTs (24, 150), whereas other work has found evidence that the other budding-yeast kinesin-5 motor, Kip1, stabilizes spindle MTs (109). Because the effect on MT dynamics appears to be not similar for all kinesin-5s, and to avoid introducing additional unknown model parameters, we assumed that all motor or cross-linker species stabilize MTs in the same way.

Previous simulation models have implemented rules for motor/cross-linker binding kinetics that do not always satisfy the principle of detailed balance for single binding/unbinding events. We computed the full filament pair partition function to ensure that cross-linker/motor kinetics followed the correct statistical mechanical rules (115, 116, 118). Attachment/detachment occurs for either head individually, so the motors/cross-linkers can have zero, one, or two heads bound. The binding and unbinding rates were chosen to ensure that the correct equilibrium distribution of bound motors/cross-linkers was recovered for passive cross-linkers and to allow force-dependent binding kinetics. Unbound motors/cross-linkers freely diffuse in the nucleoplasm (151). The motors/cross-linkers do not sterically interact with each other while either free or bound. Bound motors/cross-linkers exert forces as harmonic springs if they stretch/compress away from their rest length (152, 153), causing forces and torques on MTs to which they are bound.

We modeled passive cross-linkers and both plus end– and minus end–directed cross-linking motors with a force-velocity relation. For passive cross-linkers, both bound heads diffused along MTs in a force-dependent manner. For cross-linking motors, each motor head translocates in the appropriate direction with speed depending on the force f_{fl} exerted on the motor along the MT in the direction opposing the motor’s motion. The motor force-velocity relation is linear for simplicity and goes to zero at the motor stall force. A single motor head unbinds upon reaching

the plus end of either of the two MTs to which it is attached, whereupon it can rebind. A passive cross-linker head pauses if it reaches the end of an MT. For further model details and parameter values, see the Supplementary Materials.

Experimental methods

Experimental design.

The experiments for this work included fluorescence light microscopy measurements of SPB separation during spindle assembly, metaphase spindle length, and measurements of SPB diffusion in the absence of MTs. Our objectives were to determine the distribution of metaphase spindle lengths and the SPB diffusion coefficient in *S. pombe* cells (strains are described in the Supplementary Materials). For both objectives, we measured fluorescently tagged SPBs and quantified their movements, as described below. We did not apply any randomization or blinding because these measurements did not involve comparisons between two sets of data. The sample size was selected to be 20 to 30 cells for each measurement to obtain reasonable numbers of these time-intensive measurements. We stopped data collection once the sample size was reached; all data from each experiment were used in our analysis, and no outliers were excluded.

Spindle length.

The images of spindle elongation shown in Fig. 1 were taken using cell preparation and confocal imaging, as previously described (71, 119). Images are maximum-intensity projections. The measurements of spindle length shown in Fig. 2 (B and C) were taken using cell preparation, wide-field imaging, and three-dimensional SPB tracking, as previously described (71). Spindle length distributions of Fig. 2C were obtained by pooling length measurements beginning 5 min after the first recorded observation of the spindle being longer than 1.1 μm .

SPB diffusion.

We used fission-yeast cells with cold-sensitive β -tubulin and green fluorescent protein–tagged SPBs and a *cen2* centromere marker (71, 84). Cells were grown on YES agar plates at 32°C until small colonies started to form. Cells were then cold-treated for 7 to 9 hours at 17°C to synchronize the cells in mitosis and then suspended in growth medium containing methyl-2-benzimidazolecarbamate (MBC) to prevent repolymerization of MTs upon warming. Several small colonies were collected with a toothpick and suspended on a lectin-coated cover glass in YES + 444 μM MBC. The cover glass was then left at 17°C for a minimum of 30 min while cells settled and adhered to the lectins. Loose cells were washed off with YES + MBC; cover glass was mounted with double-sided tape on a glass slide with YES + MBC.

Imaging and analysis were performed as previously described (71). We collected seven or nine focal planes 0.3 μm apart in focus every 4 s. Data were analyzed from 26 cells to determine three-dimensional separation of the SPBs over time. All nonoverlapping time intervals were treated as independent samples. We determined the mean of the squared displacement for each time interval, with error bars representing the SE of the mean, calculated as the SD of the sample set at each time divided by the sample size at that time. We then performed a linear least-squares fit and used the slope of the mean-squared deviation curve equal to 6D for three-dimensional diffusion (fig. S1). The fit gives a relative diffusion coefficient between the two SPBs of $6 \times 10^{-4} \mu\text{m}^2/\text{s}$.

Statistical analysis

The statistical methods used in this study are described in detail in the Supplementary Materials.

SUPPLEMENTARY MATERIALS

Supplementary material for this article is available at <http://advances.sciencemag.org/cgi/content/full/3/1/e1601603/DC1>

Supplementary Materials and Methods

table S1. MT and SPB parameters.

table S2. Motor and cross-linker parameters.

table S3. Parameters varied in model optimization.

table S4. Parameters altered for cross-linker-only model.

table S5. Strains used in this study.

video S1. Simulation of the full model with reference parameter set.

video S2. Simulation of the model with short tether connecting MT minus ends to SPBs.

video S3. Simulation of the model with altered kinesin-5 bidirectionality.

video S4. Simulation of the model with a low kinesin-14 number and a low cross-linker number.

video S5. Simulation of the model with a low kinesin-5 number and a high kinesin-14 number.

video S6. Simulation of the model with a high kinesin-5 number and a low kinesin-14 number.

fig. S1. Results of SPB diffusion measurements.

fig. S2. Individual simulations of the model with simulated deletions of single species from Fig. 3 (A and B).

fig. S3. Individual simulations of the model lacking stabilization of MT dynamics by motors and cross-linkers from Fig. 3A.

fig. S4. Individual simulations of the model with varying kinesin-5 unbinding load sensitivity from Fig. 3 (C and D).

fig. S5. Individual simulations of the model with varying kinesin-14 unbinding load sensitivity from Fig. 3 (C and D).

fig. S6. Individual simulations of the model with varying cross-linker unbinding load sensitivity from Fig. 3 (C and D).

fig. S7. Individual simulations of the model with varying length of the tether linking MT minus ends to SPBs from Fig. 3 (E and F).

fig. S8. Individual simulations of the model with altered kinesin-5 direction reversal from Fig. 3 (G and H).

fig. S9. Individual simulations of the model with varying kinesin-14 and cross-linker numbers from Fig. 5B.

fig. S10. Individual simulations of the model with varying kinesin-5 and kinesin-14 numbers from Fig. 5C.

REFERENCES AND NOTES

- J. R. McIntosh, M. I. Molodtsov, F. I. Ataullakhanov, Biophysics of mitosis. *Q. Rev. Biophys.* **45**, 147–207 (2012).
- S. Petry, Mechanisms of mitotic spindle assembly. *Annu. Rev. Biochem.* **85**, 659–683 (2016).
- E. W. Taylor, Dynamics of spindle formation and its inhibition by chemicals. *J. Biophys. Biochem. Cytol.* **6**, 193–196 (1959).
- A. P. Enos, N. R. Morris, Mutation of a gene that encodes a kinesin-like protein blocks nuclear division in *A. nidulans*. *Cell* **60**, 1019–1027 (1990).
- I. Hagan, M. Yanagida, Novel potential mitotic motor protein encoded by the fission yeast *cut7* gene. *Nature* **347**, 563–566 (1990).
- I. Hagan, M. Yanagida, Kinesin-related cut 7 protein associates with mitotic and meiotic spindles in fission yeast. *Nature* **356**, 74–76 (1992).
- M. A. Hoyt, L. He, K. K. Loo, W. S. Saunders, Two *Saccharomyces cerevisiae* kinesin-related gene products required for mitotic spindle assembly. *J. Cell Biol.* **118**, 109–120 (1992).
- W. S. Saunders, M. A. Hoyt, Kinesin-related proteins required for structural integrity of the mitotic spindle. *Cell* **70**, 451–458 (1992).
- G. Östergren, Considerations on some elementary features of mitosis. *Hereditas* **36**, 1–18 (1950).
- T. S. Hays, D. Wise, E. D. Salmon, Traction force on a kinetochore at metaphase acts as a linear function of kinetochore fiber length. *J. Cell Biol.* **93**, 374–382 (1982).
- A. L. Pidoux, M. LeDizet, W. Z. Cande, Fission yeast *pk11* is a kinesin-related protein involved in mitotic spindle function. *Mol. Biol. Cell* **7**, 1639–1655 (1996).
- W. Saunders, V. Lengyel, M. A. Hoyt, Mitotic spindle function in *Saccharomyces cerevisiae* requires a balance between different types of kinesin-related motors. *Mol. Biol. Cell* **8**, 1025–1033 (1997).
- K. Nabeshima, T. Nakagawa, A. F. Straight, A. Murray, Y. Chikashige, Y. M. Yamashita, Y. Hiraoka, M. Yanagida, Dynamics of centromeres during metaphase–anaphase transition in fission yeast: Dis1 is implicated in force balance in metaphase bipolar spindle. *Mol. Biol. Cell* **9**, 3211–3225 (1998).
- G. Goshima, S. Saitoh, M. Yanagida, Proper metaphase spindle length is determined by centromere proteins Mis12 and Mis6 required for faithful chromosome segregation. *Genes Dev.* **13**, 1664–1677 (1999).

15. F. Severin, B. Habermann, T. Huffaker, T. Hyman, Stu2 promotes mitotic spindle elongation in anaphase. *J. Cell Biol.* **153**, 435–442 (2001).
16. I. M. Tolić-Nørrelykke, L. Sacconi, G. Thon, F. S. Pavone, Positioning and elongation of the fission yeast spindle by microtubule-based pushing. *Curr. Biol.* **14**, 1181–1186 (2004).
17. D. C. Bouck, K. Bloom, Pericentric chromatin is an elastic component of the mitotic spindle. *Curr. Biol.* **17**, 741–748 (2007).
18. A. D. Stephens, R. A. Haggerty, P. A. Vasquez, L. Vicci, C. E. Snider, F. Shi, C. Quammen, C. Mullins, J. Haase, R. M. Taylor, J. S. Verdaasdonk, M. R. Falvo, Y. Jin, M. G. Forest, K. Bloom, Pericentric chromatin loop function as a nonlinear spring in mitotic force balance. *J. Cell Biol.* **200**, 757–772 (2013).
19. V. Syrovatkina, C. Fu, P. T. Tran, Antagonistic spindle motors and MAPs regulate metaphase spindle length and chromosome segregation. *Curr. Biol.* **23**, 2423–2429 (2013).
20. J. Costa, C. Fu, V. M. Khare, P. T. Tran, csi2p modulates microtubule dynamics and organizes the bipolar spindle for chromosome segregation. *Mol. Biol. Cell* **25**, 3900–3908 (2014).
21. F. Zheng, T. Li, D.-y. Jin, V. Syrovatkina, K. Scheffler, P. T. Tran, C. Fu, Csi1p recruits alp7p/TACC to the spindle pole bodies for bipolar spindle formation. *Mol. Biol. Cell* **25**, 2750–2760 (2014).
22. V. Syrovatkina, P. T. Tran, Loss of kinesin-14 results in aneuploidy via kinesin-5-dependent microtubule protrusions leading to chromosome cut. *Nat. Commun.* **6**, 7322 (2015).
23. M. K. Gardner, C. G. Pearson, B. L. Sprague, T. R. Zarzar, K. Bloom, E. D. Salmon, D. J. Odde, Tension-dependent regulation of microtubule dynamics at kinetochores can explain metaphase congression in yeast. *Mol. Biol. Cell* **16**, 3764–3775 (2005).
24. M. K. Gardner, D. C. Bouck, L. V. Paliulis, J. B. Meehl, E. T. O'Toole, J. Haase, A. Soubry, A. P. Joglekar, M. Winey, E. D. Salmon, K. Bloom, D. J. Odde, Chromosome congression by kinesin-5 motor-mediated disassembly of longer kinetochore microtubules. *Cell* **135**, 894–906 (2008).
25. J. M. Chacón, S. Mukherjee, B. M. Schuster, D. J. Clarke, M. K. Gardner, Pericentromere tension is self-regulated by spindle structure in metaphase. *J. Cell Biol.* **205**, 313–324 (2014).
26. A. J. Hepperla, P. T. Willey, C. E. Coombes, B. M. Schuster, M. Gerami-Nejad, M. McClellan, S. Mukherjee, J. Fox, M. Winey, D. J. Odde, E. O'Toole, M. K. Gardner, Minus-end-directed kinesin-14 motors align antiparallel microtubules to control metaphase spindle length. *Dev. Cell* **31**, 61–72 (2014).
27. J. J. Ward, H. Roque, C. Antony, F. Nédélec, Mechanical design principles of a mitotic spindle. *eLife* **3**, e03398 (2014).
28. E. N. Cytrynbaum, J. M. Scholey, A. Mogilner, A force balance model of early spindle pole separation in *Drosophila* embryos. *Biophys. J.* **84**, 757–769 (2003).
29. E. N. Cytrynbaum, P. Sommi, I. Brust-Mascher, J. M. Scholey, A. Mogilner, Early spindle assembly in *Drosophila* embryos: Role of a force balance involving cytoskeletal dynamics and nuclear mechanics. *Mol. Biol. Cell* **16**, 4967–4981 (2005).
30. R. Wollman, G. Civelekoglu-Scholey, J. M. Scholey, A. Mogilner, Reverse engineering of force integration during mitosis in the *Drosophila* embryo. *Mol. Syst. Biol.* **4**, 195 (2008).
31. G. Civelekoglu-Scholey, L. Tao, I. Brust-Mascher, R. Wollman, J. M. Scholey, Prometaphase spindle maintenance by an antagonistic motor-dependent force balance made robust by a disassembling lamin-B envelope. *J. Cell Biol.* **188**, 49–68 (2010).
32. R. G. H. P. van Heesbeen, M. E. Tanenbaum, R. H. Medema, Balanced activity of three mitotic motors is required for bipolar spindle assembly and chromosome segregation. *Cell Rep.* **8**, 948–956 (2014).
33. F. J. Nédélec, T. Surrey, A. C. Maggs, S. Leibler, Self-organization of microtubules and motors. *Nature* **389**, 305–308 (1997).
34. T. Surrey, F. Nédélec, S. Leibler, E. Karsenti, Physical properties determining self-organization of motors and microtubules. *Science* **292**, 1167–1171 (2001).
35. F. Nédélec, Computer simulations reveal motor properties generating stable antiparallel microtubule interactions. *J. Cell Biol.* **158**, 1005–1015 (2002).
36. W. E. Channels, F. J. Nédélec, Y. Zheng, P. A. Iglesias, Spatial regulation improves antiparallel microtubule overlap during mitotic spindle assembly. *Biophys. J.* **94**, 2598–2609 (2008).
37. C. Hentrich, T. Surrey, Microtubule organization by the antagonistic mitotic motors kinesin-5 and kinesin-14. *J. Cell Biol.* **189**, 465–480 (2010).
38. J. Pringle, A. Muthukumar, A. Tan, L. Crankshaw, L. Conway, J. L. Ross, Microtubule organization by kinesin motors and microtubule crosslinking protein MAP65. *J. Phys. Condens. Matter* **25**, 374103 (2013).
39. L. Laan, N. Pavin, J. Husson, G. Romet-Lemonne, M. van Duijn, M. P. López, R. D. Vale, F. Jülicher, S. L. Reck-Peterson, M. Dogterom, Cortical dynein controls microtubule dynamics to generate pulling forces that position microtubule asters. *Cell* **148**, 502–514 (2012).
40. N. Pavin, L. Laan, R. Ma, M. Dogterom, F. Jülicher, Positioning of microtubule organizing centers by cortical pushing and pulling forces. *New J. Phys.* **14**, 105025 (2012).
41. T. Sanchez, D. T. N. Chen, S. J. DeCamp, M. Heymann, Z. Dogic, Spontaneous motion in hierarchically assembled active matter. *Nature* **491**, 431–434 (2012).
42. H. Baumann, T. Surrey, Motor-mediated cortical versus astral microtubule organization in lipid-monolayered droplets. *J. Biol. Chem.* **289**, 22524–22535 (2014).
43. G. Henkin, S. J. DeCamp, D. T. N. Chen, T. Sanchez, Z. Dogic, Tunable dynamics of microtubule-based active isotropic gels. *Philos. Trans. R. Soc. London Ser. A* **372**, 20140142 (2014).
44. R. Ma, L. Laan, M. Dogterom, N. Pavin, F. Jülicher, General theory for the mechanics of confined microtubule asters. *New J. Phys.* **16**, 013018 (2014).
45. M. vleugel, S. Roth, C. F. Groenendijk, M. Dogterom, Reconstitution of basic mitotic spindles in spherical emulsion droplets. *J. Vis. Exp.* **2016**, e54278 (2016).
46. A. Mogilner, E. Craig, Towards a quantitative understanding of mitotic spindle assembly and mechanics. *J. Cell Sci.* **123**, 3435–3445 (2010).
47. G. Civelekoglu-Scholey, D. Cimini, Modelling chromosome dynamics in mitosis: A historical perspective on models of metaphase and anaphase in eukaryotic cells. *Interface Focus* **4**, 20130073 (2014).
48. I. Brust-Mascher, G. Civelekoglu-Scholey, M. Kwon, A. Mogilner, J. M. Scholey, Model for anaphase B: Role of three mitotic motors in a switch from poleward flux to spindle elongation. *Proc. Natl. Acad. Sci. U.S.A.* **101**, 15938–15943 (2004).
49. G. Goshima, R. Wollman, N. Stuurman, J. M. Scholey, R. D. Vale, Length control of the metaphase spindle. *Curr. Biol.* **15**, 1979–1988 (2005).
50. I. Brust-Mascher, G. Civelekoglu-Scholey, J. M. Scholey, Mechanism for anaphase B: Evaluation of “slide-and-cluster” versus “slide-and-flux-or-elongate” models. *Biophys. J.* **108**, 2007–2018 (2015).
51. D. Johann, D. Goswami, K. Kruse, Generation of stable overlaps between antiparallel filaments. *Phys. Rev. Lett.* **115**, 118103 (2015).
52. D. Johann, D. Goswami, K. Kruse, Assembly of bipolar microtubule structures by passive cross-linkers and molecular motors. *Phys. Rev. E* **93**, 062415 (2016).
53. S. C. Schaffner, J. V. José, Biophysical model of self-organized spindle formation patterns without centrosomes and kinetochores. *Proc. Natl. Acad. Sci. U.S.A.* **103**, 11166–11171 (2006).
54. K. S. Burbank, T. J. Mitchison, D. S. Fisher, Slide-and-cluster models for spindle assembly. *Curr. Biol.* **17**, 1373–1383 (2007).
55. Q. Chen, D. Y. Li, K. Oiwa, The coordination of protein motors and the kinetic behavior of microtubule—A computational study. *Biophys. Chem.* **129**, 60–69 (2007).
56. M. E. Janson, R. Loughlin, I. Loïdice, C. Fu, D. Brunner, F. J. Nédélec, P. T. Tran, Crosslinkers and motors organize dynamic microtubules to form stable bipolar arrays in fission yeast. *Cell* **128**, 357–368 (2007).
57. R. J. Hawkins, S. H. Tindemans, B. M. Mulder, Model for the orientational ordering of the plant microtubule cortical array. *Phys. Rev. E* **82**, 011911 (2010).
58. F. Ziebert, M. Vershinin, S. P. Gross, I. S. Aranson, Collective alignment of polar filaments by molecular motors. *Eur. Phys. J. E Soft Matter* **28**, 401–409 (2009).
59. A. Chakravarty, L. Howard, D. A. Compton, A mechanistic model for the organization of microtubule asters by motor and non-motor proteins in a mammalian mitotic extract. *Mol. Biol. Cell* **15**, 2116–2132 (2004).
60. E. N. Cytrynbaum, V. Rodionov, A. Mogilner, Computational model of dynein-dependent self-organization of microtubule asters. *J. Cell Sci.* **117**, 1381–1397 (2004).
61. M. Bjerknes, Physical theory of the orientation of astral mitotic spindles. *Science* **234**, 1413–1416 (1986).
62. S. W. Grill, J. Howard, E. Schäffer, E. H. K. Stelzer, A. A. Hyman, The distribution of active force generators controls mitotic spindle position. *Science* **301**, 518–521 (2003).
63. S. W. Grill, K. Kruse, F. Jülicher, Theory of mitotic spindle oscillations. *Phys. Rev. Lett.* **94**, 108104 (2005).
64. J. Howard, Elastic and damping forces generated by confined arrays of dynamic microtubules. *Phys. Biol.* **3**, 54–66 (2006).
65. C. Kozłowski, M. Srayko, F. Nédélec, Cortical microtubule contacts position the spindle in *C. elegans* embryos. *Cell* **129**, 499–510 (2007).
66. C. Garzon-Coral, H. A. Fantana, J. Howard, A force-generating machinery maintains the spindle at the cell center during mitosis. *Science* **352**, 1124–1127 (2016).
67. B. Rubinstein, K. Larripa, P. Sommi, A. Mogilner, The elasticity of motor-microtubule bundles and shape of the mitotic spindle. *Phys. Biol.* **6**, 016005 (2009).
68. G. Goshima, J. M. Scholey, Control of mitotic spindle length. *Annu. Rev. Cell Dev. Biol.* **26**, 21–57 (2010).
69. R. Loughlin, J. D. Wilbur, F. J. McNally, F. J. Nédélec, R. Heald, Katanin contributes to interspecies spindle length scaling in *Xenopus*. *Cell* **147**, 1397–1407 (2011).
70. J. Brugués, D. Needleman, Physical basis of spindle self-organization. *Proc. Natl. Acad. Sci. U.S.A.* **111**, 18496–18500 (2014).
71. Z. R. Gergely, A. Crapo, L. E. Hough, J. R. McIntosh, M. D. Betterton, Kinesin-8 effects on mitotic microtubule dynamics contribute to spindle function in fission yeast. *Mol. Biol. Cell* **27**, 3490–3514 (2016).
72. R. Loughlin, R. Heald, F. Nédélec, A computational model predicts *Xenopus* meiotic spindle organization. *J. Cell Biol.* **191**, 1239–1249 (2010).

73. S. Petry, C. Pugieux, F. J. Nédélec, R. D. Vale, Augmin promotes meiotic spindle formation and bipolarity in *Xenopus* egg extracts. *Proc. Natl. Acad. Sci. U.S.A.* **108**, 14473–14478 (2011).
74. V. Magidson, R. Paul, N. Yang, J. G. Ault, C. B. O'Connell, I. Tikhonenko, B. F. McEwen, A. Mogilner, A. Khodjakov, Adaptive changes in the kinetochore architecture facilitate proper spindle assembly. *Nat. Cell Biol.* **17**, 1134–1144 (2015).
75. B. L. Sprague, C. G. Pearson, P. S. Maddox, K. S. Bloom, E. D. Salmon, D. J. Odde, Mechanisms of microtubule-based kinetochore positioning in the yeast metaphase spindle. *Biophys. J.* **84**, 3529–3546 (2003).
76. C. G. Pearson, M. K. Gardner, L. V. Paliulis, E. D. Salmon, D. J. Odde, K. Bloom, Measuring nanometer scale gradients in spindle microtubule dynamics using model convolution microscopy. *Mol. Biol. Cell* **17**, 4069–4079 (2006).
77. G. Gay, T. Courtheoux, C. Reyes, S. Tournier, Y. Gachet, A stochastic model of kinetochore–microtubule attachment accurately describes fission yeast chromosome segregation. *J. Cell Biol.* **196**, 757–774 (2012).
78. K. E. Sawin, P. T. Tran, Cytoplasmic microtubule organization in fission yeast. *Yeast* **23**, 1001–1014 (2006).
79. I. M. Tolić-Norrelykke, Force and length regulation in the microtubule cytoskeleton: Lessons from fission yeast. *Curr. Opin. Cell Biol.* **22**, 21–28 (2010).
80. R. Ding, K. L. McDonald, J. R. McIntosh, Three-dimensional reconstruction and analysis of mitotic spindles from the yeast, *Schizosaccharomyces pombe*. *J. Cell Biol.* **120**, 141–151 (1993).
81. C. L. Troxell, M. A. Sweezy, R. R. West, K. D. Reed, B. D. Carson, A. L. Pidoux, W. Z. Cande, J. R. McIntosh, *pk1⁺* and *k1p2⁺*: Two kinesins of the Kar3 subfamily in fission yeast perform different functions in both mitosis and meiosis. *Mol. Biol. Cell* **12**, 3476–3488 (2001).
82. M. J. Sagolla, S. Uzawa, W. Z. Cande, Individual microtubule dynamics contribute to the function of mitotic and cytoplasmic arrays in fission yeast. *J. Cell Sci.* **116**, 4891–4903 (2003).
83. A. Yamashita, M. Sato, A. Fujita, M. Yamamoto, T. Toda, The roles of fission yeast *ase1* in mitotic cell division, meiotic nuclear oscillation, and cytokinesis checkpoint signaling. *Mol. Biol. Cell* **16**, 1378–1395 (2005).
84. E. L. Grishchuk, J. R. McIntosh, Microtubule depolymerization can drive poleward chromosome motion in fission yeast. *EMBO J.* **25**, 4888–4896 (2006).
85. S. V. Bratman, F. Chang, Stabilization of overlapping microtubules by fission yeast CLASP. *Dev. Cell* **13**, 812–827 (2007).
86. A. S. Rodriguez, A. N. Killilea, J. Batac, J. Filopei, D. Simeonov, I. Lin, J. L. Paluh, Protein complexes at the microtubule organizing center regulate bipolar spindle assembly. *Cell Cycle* **7**, 1246–1253 (2008).
87. C. Fu, J. J. Ward, I. Loidice, G. Velve-Casquillas, F. J. Nedelec, P. T. Tran, Phospho-regulated interaction between kinesin-6 Klp9p and microtubule bundler Ase1p promotes spindle elongation. *Dev. Cell* **17**, 257–267 (2009).
88. D.-U. Kim, J. Hayles, D. Kim, W. Wood, H.-O. Park, M. Won, H.-S. Yoo, T. Duhig, M. Nam, G. Palmer, S. Han, L. Jeffery, S.-T. Baek, H. Lee, Y. S. Shim, M. Lee, L. Kim, K.-S. Heo, E. J. Noh, A.-R. Lee, Y.-J. Jang, K.-S. Chung, S.-J. Choi, J.-Y. Park, Y. Park, H. M. Kim, S.-K. Park, H.-J. Park, E.-J. Kang, H. B. Kim, H.-S. Kang, H.-M. Park, K. Kim, K. Song, K. B. Song, P. Nurse, K.-L. Hoe, Analysis of a genome-wide set of gene deletions in the fission yeast *Schizosaccharomyces pombe*. *Nat. Biotechnol.* **28**, 617–623 (2010).
89. K.-S. Hsu, T. Toda, Ndc80 internal loop interacts with Dis1/TOG to ensure proper kinetochore-spindle attachment in fission yeast. *Curr. Biol.* **21**, 214–220 (2011).
90. S. H. Choi, D. McCollum, A role for metaphase spindle elongation forces in correction of merotelic kinetochore attachments. *Curr. Biol.* **22**, 225–230 (2012).
91. I. Kalinina, A. Nandi, P. Delivani, M. R. Chacón, A. H. Klemm, D. Ramunno-Johnson, A. Krull, B. Lindner, N. Pavin, I. M. Tolić-Norrelykke, Pivoting of microtubules around the spindle pole accelerates kinetochore capture. *Nat. Cell Biol.* **15**, 82–87 (2013).
92. N. H. Tang, H. Takada, K.-S. Hsu, T. Toda, The internal loop of fission yeast Ndc80 binds Alp7/TACC-Alp14/TOG and ensures proper chromosome attachment. *Mol. Biol. Cell* **24**, 1122–1133 (2013).
93. A. Carpy, K. Krug, S. Graf, A. Koch, S. Popic, S. Hauf, B. Macek, Absolute proteome and phosphoproteome dynamics during the cell cycle of *Schizosaccharomyces pombe* (Fission Yeast). *Mol. Cell. Proteomics* **13**, 1925–1936 (2014).
94. Z. T. Olmsted, A. G. Colliver, T. D. Riehman, J. L. Paluh, Kinesin-14 and kinesin-5 antagonistically regulate microtubule nucleation by γ -TuRC in yeast and human cells. *Nat. Commun.* **5**, 5339 (2014).
95. I.-J. Lee, N. Wang, W. Hu, K. Schott, J. Bähler, T. H. Giddings Jr., J. R. Pringle, L.-L. Du, J.-Q. Wu, Regulation of spindle pole body assembly and cytokinesis by the centrin-binding protein Sfi1 in fission yeast. *Mol. Biol. Cell* **25**, 2735–2749 (2014).
96. I. B. Bouhlej, M. Ohta, A. Mayeux, N. Bordes, F. Dingli, J. Boulanger, G. V. Casquillas, D. Loew, P. T. Tran, M. Sato, A. Paoletti, Cell cycle control of spindle pole body duplication and splitting by Sfi1 and Cdc31 in fission yeast. *J. Cell Sci.* **128**, 1481–1493 (2015).
97. Z. Lansky, M. Braun, A. Lüddecke, M. Schlierf, P. R. ten Wolde, M. E. Janson, S. Diez, Diffusible crosslinkers generate directed forces in microtubule networks. *Cell* **160**, 1159–1168 (2015).
98. A. E. Chmielewska, N. H. Tang, T. Toda, The hairpin region of Ndc80 is important for the kinetochore recruitment of Mph1/MP51 in fission yeast. *Cell Cycle* **15**, 740–747 (2016).
99. E. G. Sturgill, R. Ohi, Kinesin-12 differentially affects spindle assembly depending on its microtubule substrate. *Curr. Biol.* **23**, 1280–1290 (2013).
100. C. E. Walczak, I. Vernos, T. J. Mitchison, E. Karsenti, R. Heald, A model for the proposed roles of different microtubule-based motor proteins in establishing spindle bipolarity. *Curr. Biol.* **8**, 903–913 (1998).
101. E. Bucciarelli, M. G. Giansanti, S. Bonaccorsi, M. Gatti, Spindle assembly and cytokinesis in the absence of chromosomes during *Drosophila* male meiosis. *J. Cell Biol.* **160**, 993–999 (2003).
102. T. J. Mitchison, P. Maddox, J. Gaetz, A. Groen, M. Shirasu, A. Desai, E. D. Salmon, T. M. Kapoor, Roles of polymerization dynamics, opposed motors, and a tensile element in governing the length of *Xenopus* extract meiotic spindles. *Mol. Biol. Cell* **16**, 3064–3076 (2005).
103. E. Nazarova, E. O'Toole, S. Kaitna, P. Francois, M. Winey, J. Vogel, Distinct roles for antiparallel microtubule pairing and overlap during early spindle assembly. *Mol. Biol. Cell* **24**, 3238–3250 (2013).
104. J. C. Cochran, C. A. Sontag, Z. Maliga, T. M. Kapoor, J. J. Correia, S. P. Gilbert, Mechanistic analysis of the mitotic kinesin Eg5. *J. Biol. Chem.* **279**, 38861–38870 (2004).
105. M. T. Valentine, P. M. Fordyce, T. C. Krzyziak, S. P. Gilbert, S. M. Block, Individual dimers of the mitotic kinesin motor Eg5 step processively and support substantial loads in vitro. *Nat. Cell Biol.* **8**, 470–476 (2006).
106. J. Roostal, C. Henrich, P. Bieling, I. A. Telley, E. Schiebel, T. Surrey, Directional switching of the kinesin Cin8 through motor coupling. *Science* **332**, 94–99 (2011).
107. A. Gerson-Gurwitz, C. Thiede, N. Movshovich, V. Fridman, M. Podolskaya, T. Danieli, S. Lakämper, D. R. Klopfenstein, C. F. Schmidt, L. Gheber, Directionality of individual kinesin-5 Cin8 motors is modulated by loop 8, ionic strength and microtubule geometry. *EMBO J.* **30**, 4942–4954 (2011).
108. C. Thiede, V. Fridman, A. Gerson-Gurwitz, L. Gheber, C. F. Schmidt, Regulation of bi-directional movement of single kinesin-5 Cin8 molecules. *Bioarchitecture* **2**, 70–74 (2012).
109. V. Fridman, A. Gerson-Gurwitz, O. Shapira, N. Movshovich, S. Lakämper, C. F. Schmidt, L. Gheber, Kinesin-5 Kip1 is a bi-directional motor that stabilizes microtubules and tracks their plus-ends in vivo. *J. Cell Sci.* **126**, 4147–4159 (2013).
110. M. Edamatsu, Bidirectional motility of the fission yeast kinesin-5, Cut7. *Biochem. Biophys. Res. Commun.* **446**, 231–234 (2014).
111. C. J. Chen, K. Porche, I. Rayment, S. P. Gilbert, The ATPase pathway that drives the kinesin-14 Kar3Vik1 powerstroke. *J. Biol. Chem.* **287**, 36673–36682 (2012).
112. L. C. Kapitein, M. E. Janson, S. M. J. L. van den Wildenberg, C. C. Hoogenraad, C. F. Schmidt, E. J. G. Peterman, Microtubule-driven multimerization recruits ase1p onto overlapping microtubules. *Curr. Biol.* **18**, 1713–1717 (2008).
113. M. Braun, Z. Lansky, G. Fink, F. Ruhnnow, S. Diez, M. E. Janson, Adaptive braking by Ase1 prevents overlapping microtubules from sliding completely apart. *Nat. Cell Biol.* **13**, 1259–1264 (2011).
114. B. Akiyoshi, K. K. Sarangapani, A. F. Powers, C. R. Nelson, S. L. Reichow, H. Arellano-Santoyo, T. Gonen, J. A. Ranish, C. L. Asbury, S. Beggins, Tension directly stabilizes reconstituted kinetochore-microtubule attachments. *Nature* **468**, 576–579 (2010).
115. T. Gao, R. Blackwell, M. A. Glaser, M. D. Betterton, M. J. Shelley, Multiscale polar theory of microtubule and motor-protein assemblies. *Phys. Rev. Lett.* **114**, 048101 (2015).
116. T. Gao, R. Blackwell, M. A. Glaser, M. D. Betterton, M. J. Shelley, Multiscale modeling and simulation of microtubule-motor-protein assemblies. *Phys. Rev. E Stat. Nonlin. Soft Matter Phys.* **92**, 062709 (2015).
117. H.-S. Kuan, R. Blackwell, L. E. Hough, M. A. Glaser, M. D. Betterton, Hysteresis, reentrance, and glassy dynamics in systems of self-propelled rods. *Phys. Rev. E Stat. Nonlin. Soft Matter Phys.* **92**, 060501 (2015).
118. R. Blackwell, O. Sweezy-Schindler, C. Baldwin, L. E. Hough, M. A. Glaser, M. D. Betterton, Microscopic origins of anisotropic active stress in motor-driven nematic liquid crystals. *Soft Matter* **12**, 2676–2687 (2016).
119. R. Blackwell, O. Sweezy-Schindler, C. Edelmaier, Z. R. Gergely, P. J. Flynn, S. Montes, A. Crapo, A. Doostan, J. R. McIntosh, M. A. Glaser, M. D. Betterton, Contributions of microtubule dynamic instability and rotational diffusion to kinetochore capture. *Biophys. J.* [10.1016/j.bpj.2016.09.006](https://doi.org/10.1016/j.bpj.2016.09.006) (2016).
120. J. R. McIntosh, E. O'Toole, K. Zhudenkova, M. Morphew, C. Schwartz, F. I. Ataullakhanov, E. L. Grishchuk, Conserved and divergent features of kinetochores and spindle microtubule ends from five species. *J. Cell Biol.* **200**, 459–474 (2013).
121. J. Kennedy, R. Eberhart, Particle swarm optimization, in *Proceedings of the IEEE International Conference on Neural Networks, Perth, 27 November to 11 December 1995*, vol. 4, pp. 1942–1948.
122. I. Loidice, J. Staub, T. G. Setty, N.-P. T. Nguyen, A. Paoletti, P. T. Tran, Ase1p organizes antiparallel microtubule arrays during interphase and mitosis in fission yeast. *Mol. Biol. Cell* **16**, 1756–1768 (2005).

123. S. K. Vogel, N. Pavin, N. Maghelli, F. Jülicher, I. M. Tolić-Nørrelykke, Self-organization of dynein motors generates meiotic nuclear oscillations. *PLoS Biol.* **7**, e1000087 (2009).
124. M. R. Flory, M. Morphew, J. D. Joseph, A. R. Means, T. N. Davis, Pcp1p, an Spc110p-related calmodulin target at the centrosome of the fission yeast *Schizosaccharomyces pombe*. *Cell Growth Differ.* **13**, 47–58 (2002).
125. E. G. D. Muller, B. E. Snysman, I. Novik, D. W. Hailey, D. R. Gestaut, C. A. Niemann, E. T. O'Toole, T. H. Giddings Jr., B. A. Sundin, T. N. Davis, The organization of the core proteins of the yeast spindle pole body. *Mol. Biol. Cell* **16**, 3341–3352 (2005).
126. J. V. Kilmartin, P. Y. Goh, Spc110p: Assembly properties and role in the connection of nuclear microtubules to the yeast spindle pole body. *EMBO J.* **15**, 4592–4602 (1996).
127. G. H. W. Lim, G. Huber, Y. Torii, A. Hirata, J. Miller, S. Sazer, Vesicle-like biomechanics governs important aspects of nuclear geometry in fission yeast. *PLoS ONE* **2**, e948 (2007).
128. G. H. W. Lim, G. Huber, The tethered infinitesimal tori and spheres algorithm: A versatile calculator for axisymmetric problems in equilibrium membrane mechanics. *Biophys. J.* **96**, 2064–2081 (2009).
129. I. Derényi, F. Jülicher, J. Prost, Formation and interaction of membrane tubes. *Phys. Rev. Lett.* **88**, 238101 (2002).
130. K. E. Sawin, K. LeGuellec, M. Philippe, T. J. Mitchison, Mitotic spindle organization by a plus-end-directed microtubule motor. *Nature* **359**, 540–543 (1992).
131. A. Slangy, H. A. Lane, P. d'Hérin, M. Harper, M. Kress, E. A. Nigg, Phosphorylation by p34^{cdc2} regulates spindle association of human Eg5, a kinesin-related motor essential for bipolar spindle formation in vivo. *Cell* **83**, 1159–1169 (1995).
132. T. U. Mayer, T. M. Kapoor, S. J. Haggarty, R. W. King, S. L. Schreiber, T. J. Mitchison, Small molecule inhibitor of mitotic spindle bipolarity identified in a phenotype-based screen. *Science* **286**, 971–974 (1999).
133. J. Cahu, A. Ollichon, C. Hentrich, H. Schek, J. Drinjakovic, C. Zhang, A. Doherty-Kirby, G. Lajoie, T. Surrey, Phosphorylation by Cdk1 increases the binding of Eg5 to microtubules in vitro and in *Xenopus* egg extract spindles. *PLoS ONE* **3**, e3936 (2008).
134. N. P. Ferenz, A. Gable, P. Wadsworth, Mitotic functions of kinesin-5. *Semin. Cell Dev. Biol.* **21**, 255–259 (2010).
135. A. Lockhart, R. A. Cross, Kinetics and motility of the Eg5 microtubule motor. *Biochemistry* **35**, 2365–2373 (1996).
136. J. C. Cochran, J. E. Gatial III, T. M. Kapoor, S. P. Gilbert, Monastrol inhibition of the mitotic kinesin Eg5. *J. Biol. Chem.* **280**, 12658–12667 (2005).
137. Y. Shimamoto, S. Forth, T. M. Kapoor, Measuring pushing and braking forces generated by ensembles of kinesin-5 crosslinking two microtubules. *Dev. Cell* **34**, 669–681 (2015).
138. L. C. Kapitein, B. H. Kwok, J. S. Weinger, C. F. Schmidt, T. M. Kapoor, E. J. G. Peterman, Microtubule cross-linking triggers the directional motility of kinesin-5. *J. Cell Biol.* **182**, 421–428 (2008).
139. J. Cahu, T. Surrey, Motile microtubule crosslinkers require distinct dynamic properties for correct functioning during spindle organization in *Xenopus* egg extract. *J. Cell Sci.* **122**, 1295–1300 (2009).
140. M. Uteng, C. Hentrich, K. Miura, P. Bieling, T. Surrey, Poleward transport of Eg5 by dynein–dynactin in *Xenopus laevis* egg extract spindles. *J. Cell Biol.* **182**, 715–726 (2008).
141. J. Brugués, V. Nuzzo, E. Mazur, D. J. Needleman, Nucleation and transport organize microtubules in metaphase spindles. *Cell* **149**, 554–564 (2012).
142. I. Marzo, J. Naval, Antimitotic drugs in cancer chemotherapy: Promises and pitfalls. *Biochem. Pharmacol.* **86**, 703–710 (2013).
143. Y.-G. Tao, W. K. den Otter, J. T. Padding, J. K. G. Dhont, W. J. Briels, Brownian dynamics simulations of the self- and collective rotational diffusion coefficients of rigid long thin rods. *J. Chem. Phys.* **122**, 244903 (2005).
144. H. Löwen, Brownian dynamics of hard spherocylinders. *Phys. Rev. E Stat. Phys. Plasmas Fluids Relat. Interdiscip. Topics* **50**, 1232–1242 (1994).
145. E. P. Petrov, P. Schwille, Translational diffusion in lipid membranes beyond the Saffman-Delbrück approximation. *Biophys. J.* **94**, L41–L43 (2008).
146. B. Alberts, A. Johnson, J. Lewis, M. Raff, K. Roberts, P. Walter, *Molecular Biology of the Cell* (Garland Science, ed. 5, 2008).
147. M. Dogterom, B. Yurke, Measurement of the force-velocity relation for growing microtubules. *Science* **278**, 856–860 (1997).
148. M. E. Janson, M. E. de Dood, M. Dogterom, Dynamic instability of microtubules is regulated by force. *J. Cell Biol.* **161**, 1029–1034 (2003).
149. P. Bieling, I. Kronja, T. Surrey, Microtubule motility on reconstituted meiotic chromatin. *Curr. Biol.* **20**, 763–769 (2010).
150. V. Fridman, A. Gerson-Gurwitz, N. Movshovich, M. Kupiec, L. Gheber, Midzone organization restricts inter-polar microtubule plus-end dynamics during spindle elongation. *EMBO Rep.* **10**, 387–393 (2009).
151. A. Bancaud, S. Huet, N. Daigle, J. Mozziconacci, J. Beaudouin, J. Ellenberg, Molecular crowding affects diffusion and binding of nuclear proteins in heterochromatin and reveals the fractal organization of chromatin. *EMBO J.* **28**, 3785–3798 (2009).
152. K. Kawaguchi, S. Ishiwata, Nucleotide-dependent single- to double-headed binding of kinesin. *Science* **291**, 667–669 (2001).
153. A. S. Kashlina, R. J. Baskin, D. G. Cole, K. P. Wedaman, W. M. Saxton, J. M. Scholey, A bipolar kinesin. *Nature* **379**, 270–272 (1996).

Acknowledgments

Funding: This work was funded by NSF grants DMR-0847685 (to M.D.B.), DMR-1551095 (to M.D.B.), and DMR-1420736 (to M.A.G.); NIH grants K25GM110486 (to M.D.B.), R01GM104976 (to M.D.B.), and R01GM033787 (to J.R.M.); a NIST/JILA-BioFrontiers seed grant (to M.D.B.); and a fellowship provided by matching funds from the NIH/University of Colorado Biophysics Training Program (to A.L.). The use of the Janus supercomputer was supported by NSF grant CNS-0821794, and the use of the BioFrontiers computing core was supported by NIH grant 1S10OD012300. **Author contributions:** R.B., C.E., J.R.M., M.A.G., and M.D.B. formulated the model. R.B., C.E., O.S.-S., A.L., and M.A.G. wrote the simulation code. R.B., C.E., O.S.-S., and A.L. ran the model simulations. R.B., C.E., A.L., L.E.H., and M.D.B. analyzed model results. Z.R.G., A.C., and M.D.B. performed and analyzed light microscopy measurements. E.O. performed electron microscopy measurements. R.B., C.E., Z.R.G., L.E.H., J.R.M., and M.D.B. drafted the manuscript. J.R.M. and M.D.B. edited the manuscript. **Competing interests:** The authors declare that they have no competing interests. **Data and materials availability:** All data needed to evaluate the conclusions in the paper are present in the paper and/or the Supplementary Materials. All reagents, data, and computer code for this study are available on request from the authors.

Submitted 12 July 2016

Accepted 5 December 2016

Published 20 January 2017

10.1126/sciadv.1601603

Citation: R. Blackwell, C. Edelmaier, O. Sweezy-Schindler, A. Lamson, Z. R. Gergely, E. O'Toole, A. Crapo, L. E. Hough, J. R. McIntosh, M. A. Glaser, M. D. Betterton, Physical determinants of bipolar mitotic spindle assembly and stability in fission yeast. *Sci. Adv.* **3**, e1601603 (2017).

This article is published under a Creative Commons license. The specific license under which this article is published is noted on the first page.

For articles published under [CC BY](#) licenses, you may freely distribute, adapt, or reuse the article, including for commercial purposes, provided you give proper attribution.

For articles published under [CC BY-NC](#) licenses, you may distribute, adapt, or reuse the article for non-commercial purposes. Commercial use requires prior permission from the American Association for the Advancement of Science (AAAS). You may request permission by clicking [here](#).

The following resources related to this article are available online at <http://advances.sciencemag.org>. (This information is current as of January 20, 2017):

Updated information and services, including high-resolution figures, can be found in the online version of this article at:
<http://advances.sciencemag.org/content/3/1/e1601603.full>

Supporting Online Material can be found at:
<http://advances.sciencemag.org/content/suppl/2017/01/13/3.1.e1601603.DC1>

This article **cites 150 articles**, 68 of which you can access for free at:
<http://advances.sciencemag.org/content/3/1/e1601603#BIBL>

Science Advances (ISSN 2375-2548) publishes new articles weekly. The journal is published by the American Association for the Advancement of Science (AAAS), 1200 New York Avenue NW, Washington, DC 20005. Copyright is held by the Authors unless stated otherwise. AAAS is the exclusive licensee. The title *Science Advances* is a registered trademark of AAAS